

Molecular level insight into the differential oxidase and oxygenase reactivities of *de novo* *Due Ferri* proteins

Rae Ana Snyder, Susan E. Butch, Amanda J. Reig, William F. DeGrado, and Edward I. Solomon

J. Am. Chem. Soc., **Just Accepted Manuscript** • DOI: 10.1021/jacs.5b03524 • Publication Date (Web): 19 Jun 2015

Downloaded from <http://pubs.acs.org> on June 24, 2015

Just Accepted

“Just Accepted” manuscripts have been peer-reviewed and accepted for publication. They are posted online prior to technical editing, formatting for publication and author proofing. The American Chemical Society provides “Just Accepted” as a free service to the research community to expedite the dissemination of scientific material as soon as possible after acceptance. “Just Accepted” manuscripts appear in full in PDF format accompanied by an HTML abstract. “Just Accepted” manuscripts have been fully peer reviewed, but should not be considered the official version of record. They are accessible to all readers and citable by the Digital Object Identifier (DOI®). “Just Accepted” is an optional service offered to authors. Therefore, the “Just Accepted” Web site may not include all articles that will be published in the journal. After a manuscript is technically edited and formatted, it will be removed from the “Just Accepted” Web site and published as an ASAP article. Note that technical editing may introduce minor changes to the manuscript text and/or graphics which could affect content, and all legal disclaimers and ethical guidelines that apply to the journal pertain. ACS cannot be held responsible for errors or consequences arising from the use of information contained in these “Just Accepted” manuscripts.



Molecular level insight into the differential oxidase and oxygenase reactivities of *de novo Due Ferri* proteins

Rae Ana Snyder,[†] Susan E. Butch,[‡] Amanda J. Reig,^{‡,*} William F. DeGrado,^{‡,*} and Edward I. Solomon^{†,§,*}

Department of Chemistry, Stanford University, Stanford, California 94305, Department of Chemistry, Ursinus College, Collegeville, Pennsylvania 19426, Department of Pharmaceutical Chemistry, University of California San Francisco, San Francisco, California 94143 and Stanford Synchrotron Radiation Laboratory, Stanford University, SLAC, Menlo Park, California 94025

Abstract: Using the DFsc (single-chain *due ferri* peptide) scaffold, the differential oxidase and oxygenase reactivities of two 4A→4G variants, one with 2 histidines at the diiron center (G4DFsc) and the other with 3 histidines (3His-G4DFsc(Mut3)), are explored. By controlling the reaction conditions, the active form responsible for 4-aminophenol oxidase activity in both G4DFsc and 3His-G4DFsc(Mut3) is determined to be the substrate bound biferrous site. Using CD, MCD, and VTVH MCD spectroscopies, 4-aminophenol is found to bind directly to the biferrous sites of the DF proteins. In G4DFsc, 4-aminophenol increases the coordination of the biferrous site, while in 3His-G4DFsc(Mut3), the coordination number remains the same and the substrate likely replaces the additional bound histidine. This substrate binding enables a 2-electron process where 4-aminophenol is oxidized to benzoquinone imine and O₂ is reduced to H₂O₂. In contrast, only the biferrous 3His variant is found to be active in the oxygenation of *p*-anisidine to 4-nitroso-methoxybenzene. From CD, MCD and VTVH MCD, *p*-anisidine addition is found to minimally perturb the biferrous centers of both G4DFsc and 3His-G4DFsc(Mut3), indicating that this substrate binds near the biferrous site. In 3His-G4DFsc(Mut3), the coordinative saturation of one iron leads to the 2-electron reduction of O₂ at the second iron to generate an end-on hydroperoxo-Fe(III) active oxygenating species.

[†] Department of Chemistry, Stanford University

[‡] Department of Chemistry, Ursinus College

[‡] Department of Pharmaceutical Chemistry, University of California San Francisco

[§] Stanford Synchrotron Radiation Laboratory, Stanford University.

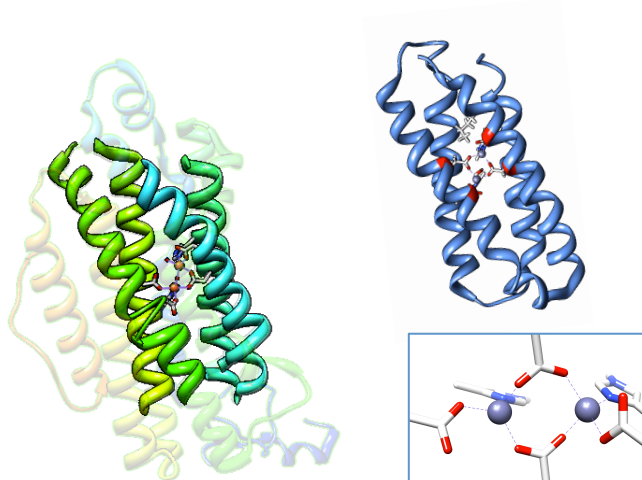
* To whom correspondence should be addressed. A.J.R.: e-mail, areig@ursinus.edu; phone, (610) 409-3383; W.F.D.: e-mail, Bill.DeGrado@ucsf.edu; phone, (415) 476-9679; E.I.S.: e-mail, edward.solomon@stanford.edu; phone, (650) 723-9104.

Introduction

Binuclear non-heme iron enzymes catalyze a variety of biologically significant reactions with relevance to biotechnology,^{1,2} environmental remediation,³ and drug design.^{4,5} The catalyzed reactions are usually O₂ dependent and generally include oxidation and oxygenation of substrates.⁵⁻⁸ Representative binuclear non-heme iron enzymes that function as oxidases include alternative oxidase (AOX) and flavin diiron protein (FDP).⁹⁻¹⁴ AOX has a diiron center that participates in the mitochondrial electron transport chain in plants and bacteria, catalyzing ubiquinol oxidation with O₂ (which is reduced to H₂O₂) and allowing for cyanide resistant respiration.¹⁴ Flavin diiron proteins are oxidases that protect anaerobes from oxidative stress.⁹⁻¹³ Among the many binuclear non-heme iron enzymes that function as oxygenases are methane monooxygenase (MMO, methane to methanol),¹⁵⁻¹⁸ toluene-4-monooxygenase (T4MO, toluene to methylphenol),¹⁹ and *p*-aminobenzoate *N*-oxygenase (AurF, *p*-aminobenzoate to *p*-nitrobenzoate)^{20,21}.

The diiron active sites of binuclear non-heme iron enzymes are coordinated to the protein by histidine and carboxylate residues and are often contained within common 4-helix bundle motifs (Figure 1).^{5-8,15,16,22-25} While a two-histidine and four-carboxylate coordination of the diiron center (two of the carboxylates bridge the ferrous centers) is observed in many cases, such as in MMO,¹⁵⁻¹⁷ ribonucleotide reductase^{5,25} and delta-9 desaturase,^{23,24} the number of coordinating histidine and carboxylate residues can vary.^{6,20,26} An additional histidine binds to one of the iron sites (3His/4-carboxylate ligand set) in AurF and *Myo*-inositol oxygenase (MIOX) has a diiron center with a four-histidine and two-carboxylate coordination.^{20,27-31} Many binuclear non-heme iron enzymes react with O₂ in their biferrous states to form activated

1
2
3 intermediates.^{5-8,32-39} MMO reacts with O₂ to form a high valent intermediate (Q) that acts as the
4
5 oxygenating species.^{18,40-42} Alternatively in AurF, a peroxy-intermediate species has been
6
7 proposed as the *N*-oxygenating species.^{29,38}
8
9
10
11
12
13
14
15
16
17
18
19
20
21
22
23
24
25
26
27
28
29
30



31
32 Figure 1: Crystal structure of ribonucleotide reductase (left) (PDB 1RIB)⁴³ with the 4-helix bundle motif
33 bolded and the NMR structure of Zn substituted DFsc (right) (PDB 2HZ8)⁴⁴. A close up of the active site
34 with 2-histidines+4-carboxylate coordination is shown in the bottom right. The 4A shown in red of the
35 NMR structure of DFsc are mutated to 4G (A10G, A14G, A43G, A47G) in G4DFsc.
36
37

38 *Due ferri* (DF) *de novo* proteins, peptides that self-assemble as 4-helix bundle units
39
40 (Figure 1, right) with binuclear non-heme iron centers, are used to model native binuclear non-
41
42 heme iron enzymes. They offer the simplicity of small molecules while still maintaining the
43
44 native protein environment.⁴⁵⁻⁴⁷ The single chain DF peptides (DFsc), a subset of DF, form
45
46 scaffolds that mimic the folding properties and asymmetry of native diiron proteins.^{48,49} The
47
48 original DFsc variant, which was constructed to contain the common 2-His/4-carboxylate ligand
49
50 set (found in ribonucleotide reductase, MMO, delta-9 desaturase, etc), displayed O₂ reaction
51
52 rates similar to natural diiron proteins.⁵⁰ In order to increase solvent and substrate accessibility, a
53
54 4A→4G variant (G4DFsc, DFsc with mutations = A10G, A14G, A43G, A47G) was made.⁵¹
55
56
57
58
59
60

1
2
3 While still retaining the 2-His/4-carboxylate ligand set, the new variant displayed a decrease in
4 the O₂ reaction rate.⁵² Additionally, a version of G4DFsc where three (rather than two) histidine
5 residues are near the diiron center (3His-G4DFsc(Mut3)) was constructed to model the ligation
6 of AurF.⁵¹ In order to incorporate the 3rd His residue at the diiron site (I100H), three additional
7 mutations (Mut3 = Y18L, I37N, and L81H) were required for protein stability.
8
9

10
11
12
13
14
15 The perturbation of G4DFsc to incorporate an additional histidine at the diiron active site
16 was found to significantly alter its reactivity.⁵¹ Our previous studies evaluated arylamine oxidase
17 and oxygenase activities of G4DFsc and 3His-G4DFsc(Mut3) using 4-aminophenol and *p*-
18 anisidine as substrates. While G4DFsc and 3His-G4DFsc(Mut3) were shown to have comparable
19 O₂ reaction rates,⁵² the activity studies revealed that G4DFsc catalyzed the oxidation of 4-
20 aminophenol, while the 3His form only had minimal activity.⁵¹ The 3His form did, however,
21 show oxygenase reactivity towards the amine group of *p*-anisidine, while G4DFsc appeared
22 inactive in this reaction. Thus, 3His-G4DFsc(Mut3) was demonstrated to be a functional model
23 of AurF.
24
25
26
27
28
29
30
31
32
33
34
35

36
37 The present study elucidates how incorporation of an additional histidine at the diiron
38 center modifies the reactivities of G4DFsc. These investigations define the active species
39 involved and give insight into the differential oxidase and oxygenase activities of 2His (G4DFsc)
40 and 3His (3His-G4DFsc(Mut3)) forms of diiron proteins. The structures and reactivities of the
41 substrate bound biferrous species are probed using near IR (NIR) circular dichroism (CD),
42 magnetic circular dichroism (MCD) and variable temperature variable field (VTVH) MCD
43 spectroscopies. NIR CD and MCD are used to probe the ferrous d → d transitions, which
44 correlate to the geometry of each Fe(II) center.⁶ VTVH MCD uses these excited state transitions
45 to study the ground state and extract information on the magnetic coupling between the two iron
46
47
48
49
50
51
52
53
54
55
56
57
58
59
60

1
2
3 sites, which correlates with the bridging ligands. This also provides the zero-field splitting (ZFS)
4
5 of the individual iron centers, which compliments the geometric information obtained from CD
6
7 and MCD spectroscopies. Based on these studies, we elucidate how the properties of substrate
8
9 binding to the biferrous sites define the differences in reactivities observed between the 2His
10
11 (G4DFsc) and the 3His (3His-G4DFsc(Mut3)) forms of *de novo* designed binuclear non-heme
12
13 iron proteins.
14
15
16
17
18
19
20
21
22
23
24
25
26
27
28
29
30
31
32
33
34
35
36
37
38
39
40
41
42
43
44
45
46
47
48
49
50
51
52
53
54
55
56
57
58
59
60

Results and Analysis.

Oxidase Activity.

Reactivity.

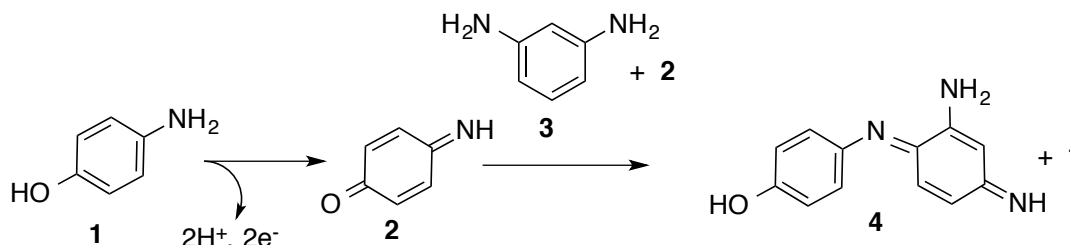


Figure 2: Two-electron oxidation of 4-aminophenol followed by coupling with *m*-phenylenediamine to form an aminoindoaniline dye.

Based on our prior studies, the biferrous G4DFsc reacts with O₂ to first form a paramagnetic species (attributed to a biferric site with only μ -1,3 carboxylate bridges, Species B) that decays into a diamagnetic species (attributed to a hydroxo-bridged antiferromagnetically coupled biferric site, Species C).⁵² However, 3His-G4DFsc(Mut3) only formed the biferric paramagnetic species B due to the additional His coordinatively saturating one iron center. In our prior studies that showed oxidase reactivity for G4DFsc, but not for the 3His form, Fe(II) was added under aerobic conditions to a solution of apo-protein and 4-aminophenol (1) in the presence of *m*-phenylenediamine (3), which couples to the oxidized product (quinone imine) (2) to yield an aminoindoaniline dye (4) with $\lambda_{\text{max}} = 486 \text{ nm}$ ($\epsilon = 13,200 \text{ cm}^{-1} \text{ M}^{-1}$) at pH 7 (Figure 2).⁵¹ The conditions of the prior studies, which allowed for the simultaneous presence of the biferric (Species B and C)⁵² and biferrous forms and may have included contributions from Fe(II) binding to the protein, complicated our ability to identify the catalytically active species. Using more controlled reaction conditions, the prior studies⁵¹ were thus extended to identify the reactive species of G4DFsc responsible for catalyzing the oxidation of 4-aminophenol, as well as address the apparent lack of activity in the 3His form.

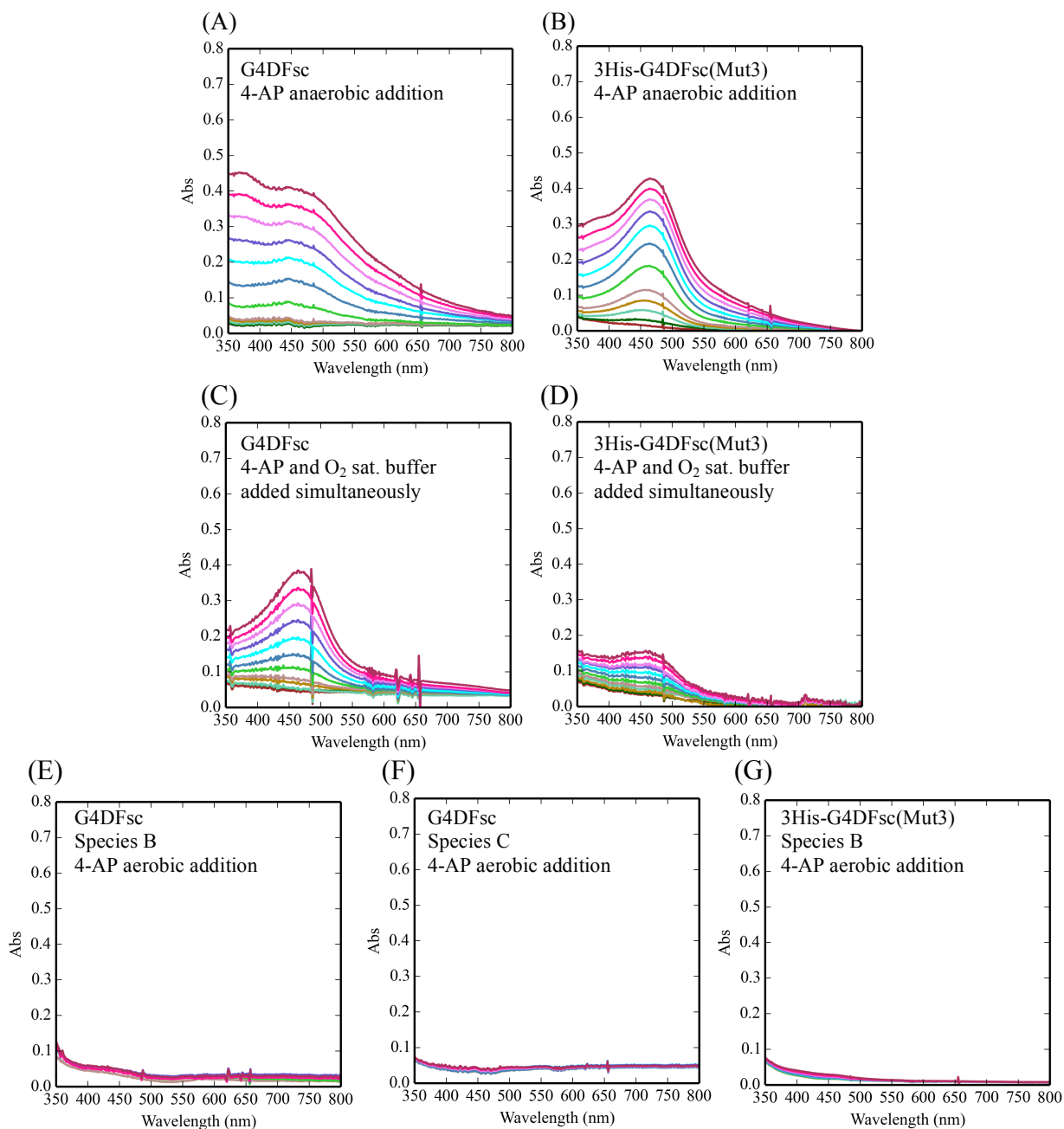


Figure 3: The oxidation of 4-aminophenol (4-AP) for various reaction conditions over 10 min. The reaction conditions include: (1) the addition of O_2 saturated buffer to biferrous G4DFsc (A) and 3His-G4DFsc(Mut3) (B) with 4-AP (in the presence of *m*-phenylenediamine) already loaded; (2) the simultaneous addition of O_2 saturated buffer and 4-AP (in the presence of *m*-phenylenediamine) to biferrous G4DFsc (C) and 3His-G4DFsc(Mut3) (D); (3) the addition of 4-AP (in the presence of *m*-phenylenediamine) to the biferric paramagnetic Species B (E) and diamagnetic Species C (F) for G4DFsc and the biferric diamagnetic Species B for 3His-G4DFsc(Mut3) (G). Aminoindolanine dye formation was used to identify the oxidation of 4-AP (see Figure 2). Final concentrations (after O_2 saturated buffer addition) were $10 \mu\text{M}$ for protein, 3.9 mM 4-aminophenol, and 10 mM *m*-phenylenediamine.

1
2
3
4
5
6
7
8
9
10
11
12
13
14
15
16
17
18
19
20
21
22
23
24
25
26
27
28
29
30
31
32
33
34
35
36
37
38
39
40
41
42
43
44
45
46
47
48
49
50
51
52
53
54
55
56
57
58
59
60

To test the biferrous forms of G4DFsc and 3His-G4DFsc(Mut3), Fe(II) was added to the apo-protein in an anaerobic environment (glove box) to exclude possible iron binding effects that may complicate the reactivity. 4-aminophenol was also added to the Fe(II) protein under anaerobic conditions and incubated for 15 min. This was followed by the anaerobic addition of *m*-phenylenediamine, and then, O₂ saturated buffer at 4 °C. Under these conditions, 4-aminophenol oxidation was observed in both G4DFsc and 3His-G4DFsc(Mut3) (Figure 3 (A) and (B)). Since these results were not consistent with our prior study, 4-aminophenol (with *m*-phenylenediamine) was also added simultaneously with O₂ saturated buffer to biferrous protein. These conditions reproduced the observations of prior studies, where the 3His form showed much reduced activity compared to G4DFsc (Figure 3 (C) and (D)). Biferric species B and C in G4DFsc, as well as the biferric form of 3His-G4DFsc(Mut3), were also tested and showed no activity (Figure 3 (E), (F) and (G)). The 4-aminophenol oxidation with both substrate loaded G4DFsc and 3His-G4DFsc(Mut3) biferrous forms produced multiple equivalents of the indoaniline dye per diiron site over time (5 eq. after 20 min, Figure S9). These data indicate that the biferrous forms of G4DFsc and 3His-G4DFsc(Mut3) are the catalytically active species and that in the case of the 3His form, substrate addition prior to oxidation is required for reactivity.

Spectroscopic definition of substrate binding.

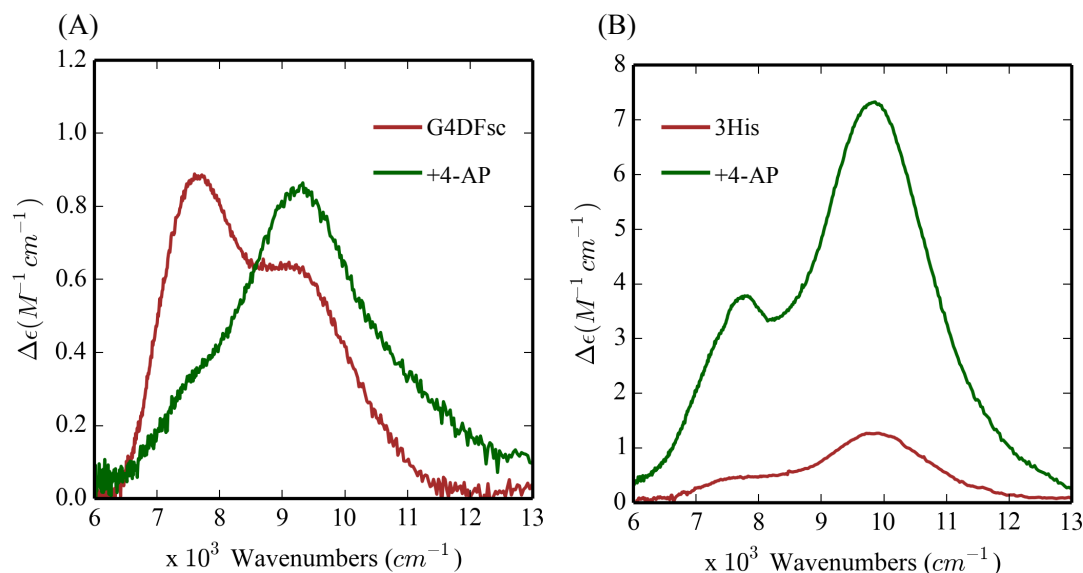


Figure 4: 4-aminophenol (4-AP) perturbation of the MCD spectra of (A) G4DFsc and (B) 3His-G4DFsc(Mut3) in the absence (red) and presence (green) of 4-aminophenol. All spectra taken at 2 K and 7 T (baseline subtracted). Protein concentrations were ~ 1 mM with 15-fold excess substrate.

To understand the effects of substrate loading on the biferrous sites, MCD and VTVH MCD spectroscopies were employed to determine the structures of the Fe(II)Fe(II) forms of these DF proteins in the presence of 4-AP. While addition of 4-aminophenol to the Fe(II)Fe(II) states of G4DFsc and 3His-G4DFsc(Mut3) only slightly perturbs their CD spectra (Figure S3), the substrate addition significantly alters the MCD spectra (Figure 4) for both DF forms. In the presence of excess 4-aminophenol (15 fold), an additional higher energy feature appears in the low temperature MCD spectrum of biferrous G4DFsc (Figure 4 (A)) and the MCD intensity significantly increases for biferrous 3His-G4DFsc(Mut3) (Figure 4 (B)). These changes indicate that 4-aminophenol is appreciably perturbing the biferrous site in each protein and likely binding to an Fe(II) center (Figure S18). The CD and MCD features for G4DFsc in the presence of 4-AP were Gaussian resolved into 3 bands at $7,540(+)$, $9,000(-)$, and $10,540(+)$ cm^{-1} in the CD spectrum, and at $7,800$, $9,100$, and $10,500$ cm^{-1} in the MCD spectrum (Figure 5 (A)). The CD

1
2
3 and MCD spectra for 3His-G4DFsc(Mut3) with excess 4-aminophenol were also resolved into 3
4
5 bands (Figure 5 (B)) that have the same signs and energies as those of the 3His form without 4-
6
7 aminophenol but with $\sim 7\times$ greater intensity with substrate bound.⁵² Note that the small shifts in
8
9 energy and narrowing of the band shapes in the MCD spectra are due to the lower temperature of
10
11 data collection. The 3 bands for the 3His form (7,400(+), 9,300(-), and 10,500(+) cm^{-1} for CD
12
13 and 7,700, 9,400, and 10,300 cm^{-1} for MCD) also have the same sign and are at very similar
14
15 energies as those for G4DFsc with 4-aminophenol bound (G4DFsc+4-AP). Biferrous 3His-
16
17 G4DFsc(Mut3) was previously described as having a 5-coordinate+6-coordinate site based on its
18
19 CD and MCD spectra, while that of G4DFsc was described as a 5-coordinate+5-coordinate site.⁵²
20
21 The similarities in energy and sign of these CD and MCD features for G4DFsc+4-AP, 3His-
22
23 G4DFsc(Mut3)+4-AP, and 3His-G4DFsc(Mut3) indicate that all three forms have equivalent
24
25 coordination environments with one 6-coordinate and one 5-coordinate trigonal bipyramidal
26
27 Fe(II) center. This would suggest that 4-aminophenol addition increases the coordination of
28
29 G4DFsc (5-coordinate+5-coordinate to 5-coordinate+6-coordinate), while maintaining 5-
30
31 coordinate+6-coordinate for 4-aminophenol bound 3His-G4DFsc(Mut3) but with a significant
32
33 perturbation of the diiron site (i.e. the increased MCD intensity).
34
35
36
37
38
39
40
41
42
43
44
45
46
47
48
49
50
51
52
53
54
55
56
57
58
59
60

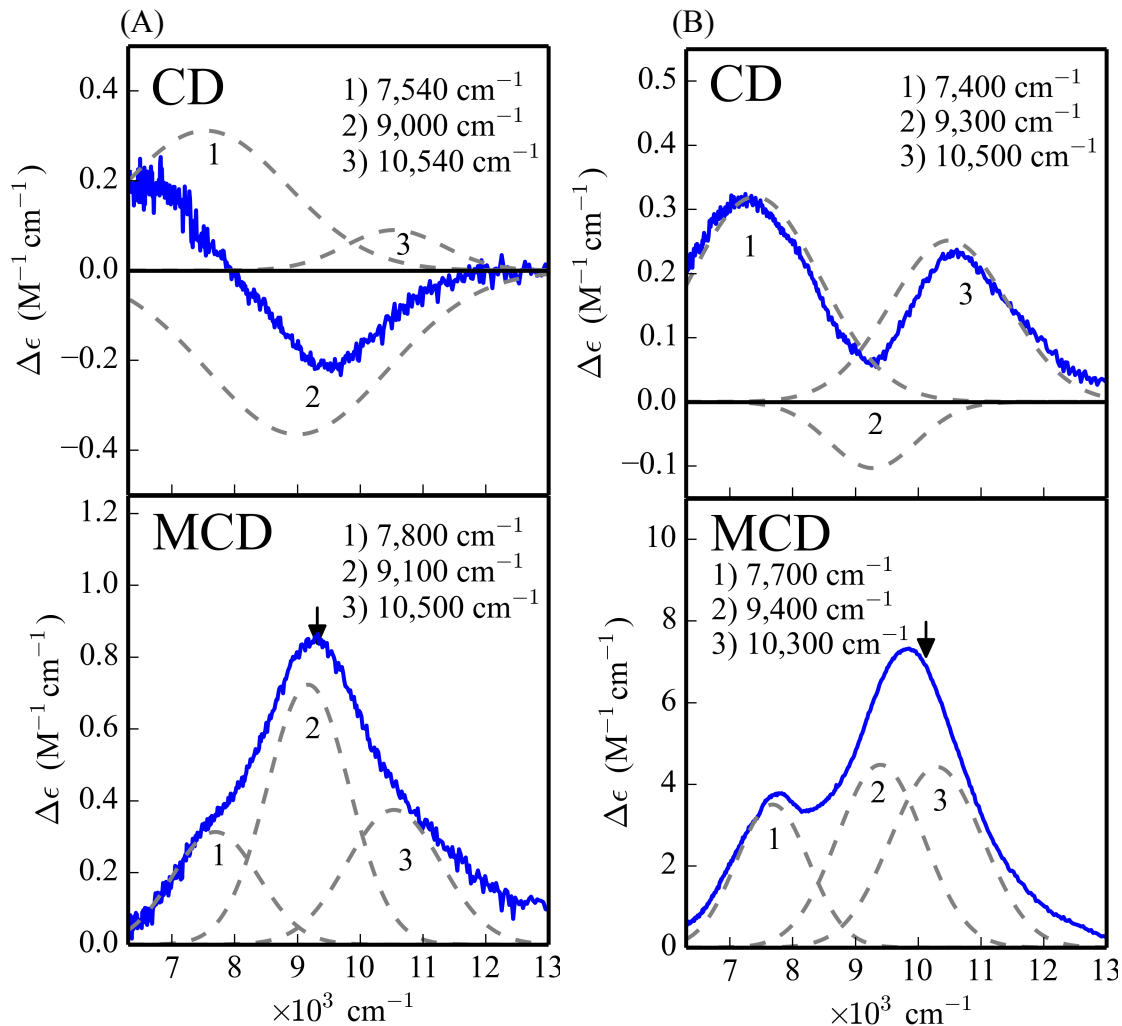


Figure 5: Gaussian resolution of the CD and MCD spectra of G4DFsc (A) and 3His-G4DFsc(Mut3) (B) with the addition of 4-aminophenol. Black arrows denote where VTVH MCD isotherms were taken. CD was taken at 4 °C. MCD was taken at 2 K and 7 T (baseline subtracted). Protein concentrations are ~1 mM with 15-fold excess substrate.

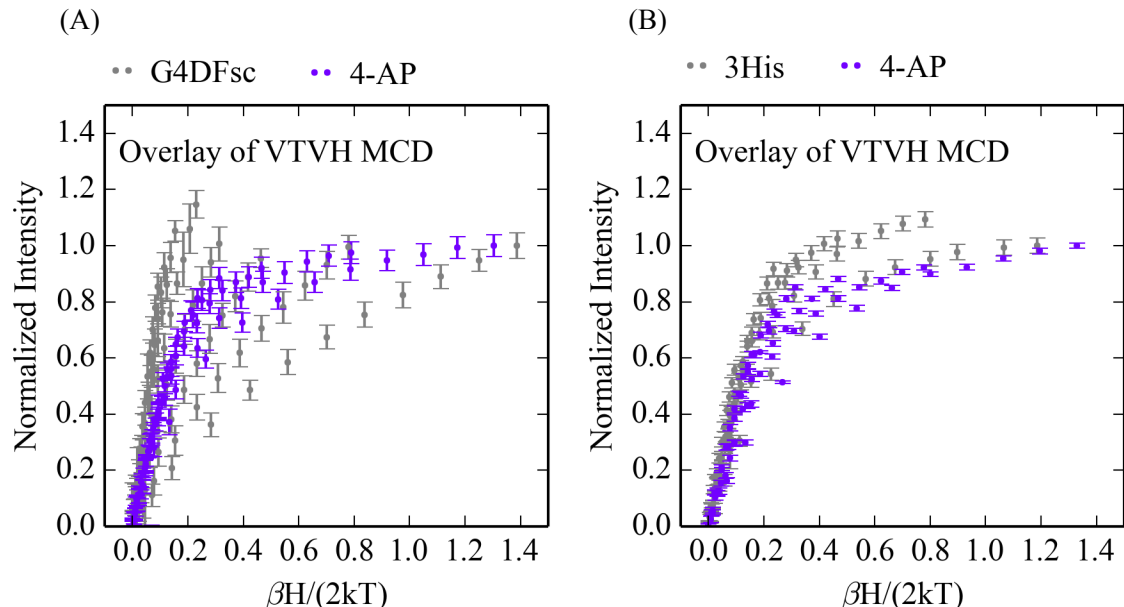


Figure 6: The effect of 4-aminophenol (4-AP) addition on VTVH MCD data. Overlay with (purple) and without (grey) 4-AP for G4DFsc at $9,100\text{ cm}^{-1}$ (A) and 3His-G4DFsc(Mut3) at $10,400\text{ cm}^{-1}$ (B). 2 K, 3 K, 5 K, 7.5 K, 10 K, 15 K, 20 K, and 25 K isotherms are shown for all data sets.

The VTVH MCD data for both G4DFsc and 3His-G4DFsc(Mut3) are perturbed with the addition of 4-aminophenol (Figure 6), which further substantiates the above results that suggest 4-aminophenol binds to these biferrous sites, in this case perturbing their ground states. Interestingly, the VTVH MCD data for G4DFsc+4-AP and 3His-G4DFsc(Mut3)+4-AP are similar to each other (Figure 7 (A)).

The spin-manifold for a biferrous system is described by the spin-Hamiltonian (eq. 1):⁶

$$H = -2J\widehat{S}_1 \cdot \widehat{S}_2 + D_1 \left(\widehat{S}_{z1}^2 - \frac{1}{3}S_1(S_1 + 1) \right) + E_1 \left(\widehat{S}_{x1}^2 - \widehat{S}_{y1}^2 \right) + D_2 \left(\widehat{S}_{z2}^2 - \frac{1}{3}S_2(S_2 + 1) \right) + E_2 \left(\widehat{S}_{x2}^2 - \widehat{S}_{y2}^2 \right) \quad (\text{eq. 1})$$

where J, D₁, D₂, E₁, and E₂ quantify the magnetic coupling between Fe1 and Fe2, and the axial and rhombic ZFS of Fe1 and Fe2, respectively. As previously described,⁶ this equation is applied to the uncoupled basis set $|S_1, S_2, M_{s1}, M_{s2}\rangle$ of Fe1 and Fe2 to obtain eigenvectors and eigenvalues from a 25x25 matrix. VTVH MCD data can be fit using a model, also previously

1
2
3 described,⁶ that expresses the MCD intensity for a non-Kramers system (i.e. the biferrrous site) as
4 a series of doublets where each doublet has an effective g-value (g_{\parallel}), rhombic ZFS (δ), and C-
5 term (A_{tot}) and B-term MCD intensities. These doublets correlate to the sublevels given by the
6 eigenvectors and eigenvalues obtained from eq. 1, and thus, allow determination of the exchange
7 coupling associated with bridging ligation and the ZFS associated with the ligand field of each
8 iron center. The VTVH MCD data for both 3His-G4DFsc(Mut3)+4-AP (Figure 7 (B)) and
9 G4DFsc+4-AP (Figure S5) were fit to the doublet model with similar parameters as described in
10 the Supporting Information. This gives a system that is antiferromagnetically coupled with
11 oppositely signed ZFS values for each Fe(II) center ($-J < 1 \text{ cm}^{-1}$, $D_1 = 5-15 \text{ cm}^{-1}$ with $(E/D)_1 =$
12 0.33 and $-D_2 = 5-15 \text{ cm}^{-1}$ with $(E/D)_2 = 0.33$, see Table 1). These parameter ranges are similar to
13 those for 3His-G4DFsc(Mut3) found previously⁵² (Table 1) that describe a weakly
14 antiferromagnetic exchange coupled site indicating μ -1,3 carboxylate bridges.
15
16
17
18
19
20
21
22
23
24
25
26
27
28
29
30
31
32
33
34
35
36
37
38
39
40
41
42
43
44
45
46
47
48
49
50
51
52
53
54
55
56
57
58
59
60

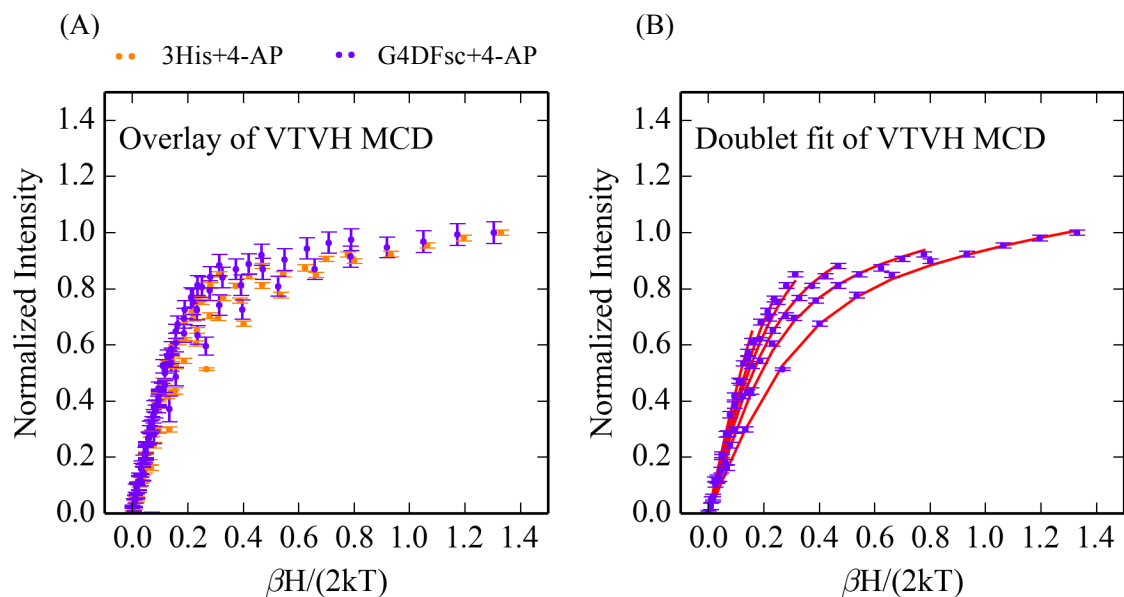


Figure 7: VTVH MCD data for biferrous G4DFsc and 3His-G4DFsc(Mut3) following 4-aminophenol addition. (A) Overlay of the VTVH MCD for G4DFsc (purple) (at $9,100\text{ cm}^{-1}$) and 3His-G4DFsc(Mut3) (orange) (at $10,400\text{ cm}^{-1}$) with addition of 4-aminophenol, and (B) Doublet fit to the VTVH MCD of 3His-G4DFsc(Mut3)+4-AP. 2 K, 3 K, 5 K, 7.5 K, 10 K, 15 K, and 20 K isotherms are shown.

Table 1: Spin-Hamiltonian parameters for G4DFsc and 3His-G4DFsc(Mut3)

		G4DFsc	3His	G4DFsc+4-AP	3His+4-AP
	$-J\text{ (cm}^{-1}\text{)}$	3-4	1-3	< 1	< 1
Spin	$D_1\text{ (cm}^{-1}\text{)}$	5-10	10-15	5-15	5-15
Hamiltonian	$(E/D)_1$	0.33	0.33	0.33	0.33
Parameters	$D_2\text{ (cm}^{-1}\text{)}$	-7 to -14	-10 to -15	-5 to -15	-5 to -15
	$(E/D)_2$	0.15	0.33	0.33	0.33

1
2
3
4
5
6 The 4-aminophenol likely binds to the Fe(II)Fe(II) site as a phenolate with the oxygen as
7 the donor atom (pKa of hydroxo group ~ 10.8). While this phenolate is likely binding to an open
8 coordinate position of the 2His DF form (G4DFsc), it appears to be replacing a ligand in the 3His
9 form (based on the increase in MCD intensity). Given the spectroscopic similarities between
10 G4DFsc+4-AP and 3His-G4DFsc(Mut3)+4-AP, as described above, we propose that the 4-
11 aminophenolate has replaced the additional active site His at position 100 in 3His-
12 G4DFsc(Mut3).
13
14
15
16
17
18
19
20
21
22
23
24
25
26
27
28
29
30
31
32
33
34
35

36 *Kinetics.*

37
38
39 The change in the MCD spectrum for both G4DFsc and 3His-G4DFsc(Mut3) upon the
40 addition of 4-aminophenol provides a spectroscopic approach to determine the rate of substrate
41 binding. A solution of 4-aminophenol (in 54% d-glycerol) was anaerobically mixed into a
42 sample of biferrous protein (also in 54% d-glycerol) in an MCD cell and frozen at different time
43 intervals. The intermediate spectrum of G4DFsc taken from a sample frozen (in liquid nitrogen)
44 at 0.5 min after addition of 4-AP (Figure 8 (A), teal) is a combination of the final spectrum (after
45 20 min, dark green) and the initial spectrum (red), and overlays with a composite spectrum
46
47
48
49
50
51
52
53
54
55
56
57
58
59
60

generated using 55-70% of the G4DFsc+4-AP final MCD spectrum and 45-30% of the G4DFsc MCD spectrum (Figure S6). Assuming a simple $A \rightarrow B$ binding scheme and using this 0.5 min

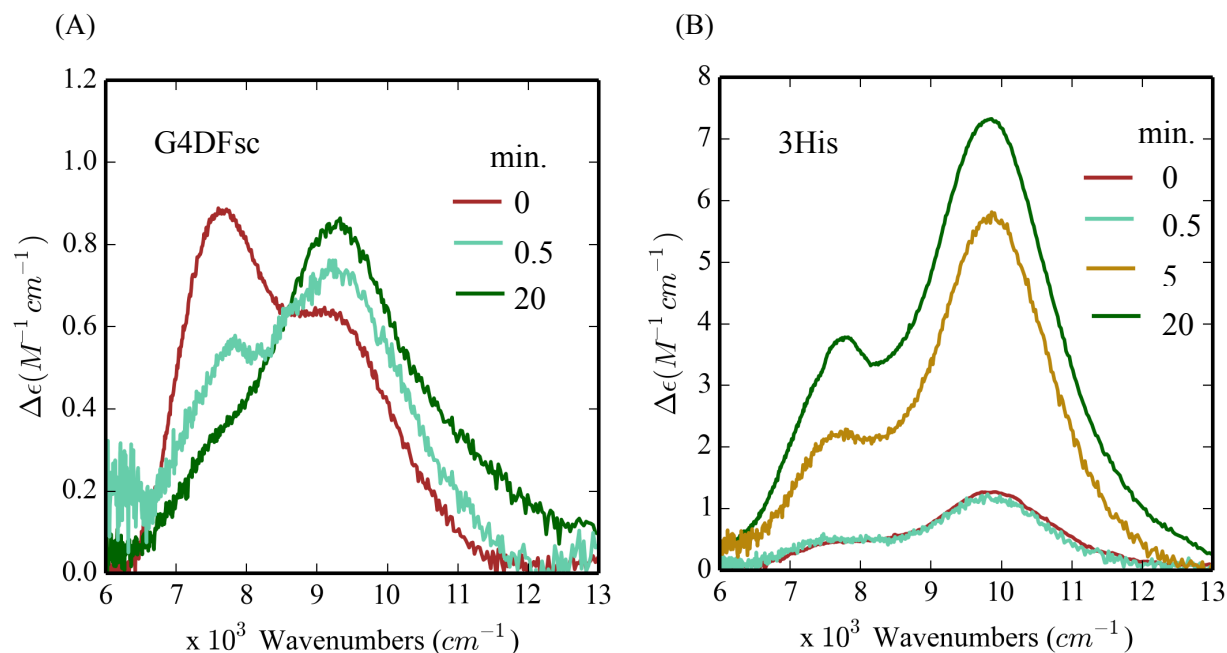


Figure 8: MCD spectra monitoring 4-aminophenol binding at different time intervals for (A) G4DFsc and (B) 3His-G4DFsc(Mut3). All time points taken at 2 K and 7 T. The 0.5 min. time interval in (A) is a composite of the initial (red) and end (dark green) spectra (30/70). The 5 min time interval in (B) has intensity consistent with a composition of the initial (red) and end (dark green) spectra (25/75).

interval spectrum, the rate of 4-aminophenol binding is estimated to be $k_B = 0.027-0.042 s^{-1}$.

While the MCD spectrum for 3His-G4DFsc(Mut3) after 4-aminophenol addition at the same intermediate time interval (0.5 min) (Figure 8 (B), teal) shows little perturbation from its initial spectrum (red), the spectrum at 5 min after 4-aminophenol addition shows an increase in intensity (dark yellow) that results in a final spectrum after 20 min (dark green). The intermediate spectrum (5 min) overlays with a composite spectrum generated using 60-75 % of the final and 40-25 % of the initial spectrum (Figure S8). As calculated above for G4DFsc, the rate for 4-aminophenol binding to 3His-G4DFsc(Mut3) is $k_B = 0.003-0.0046 s^{-1}$. These data demonstrate that 4-aminophenol binds an order of magnitude more rapidly to the biferrous site of the 2His form than to the biferrous site of the 3His DF variant. This result would be consistent

with a binding mechanism where the 4-aminophenol displaces the 3rd His at the diiron site in 3His-G4DFsc(Mut3), while simply increasing the coordination number of one Fe(II) center of the 2His form.

Based on previous studies, the rates for O₂ reactivity of the biferrous G4DFsc and 3His-G4DFsc(Mut3) forms without substrate are 0.01-0.03 s⁻¹ and 0.01-0.06 s⁻¹.⁵² Thus, the rate of O₂ oxidation is greater than the rate of substrate binding for the biferrous 3His form, but comparable for biferrous G4DFsc. These substrate binding and O₂ reaction rates thus provide an explanation for the difference in observed reactivity where the 3His form is active only when the reduced protein has been incubated with substrate leading to replacement/substitution of the 3rd active site His ligand, while incubation is not required for activity in the 2His form.

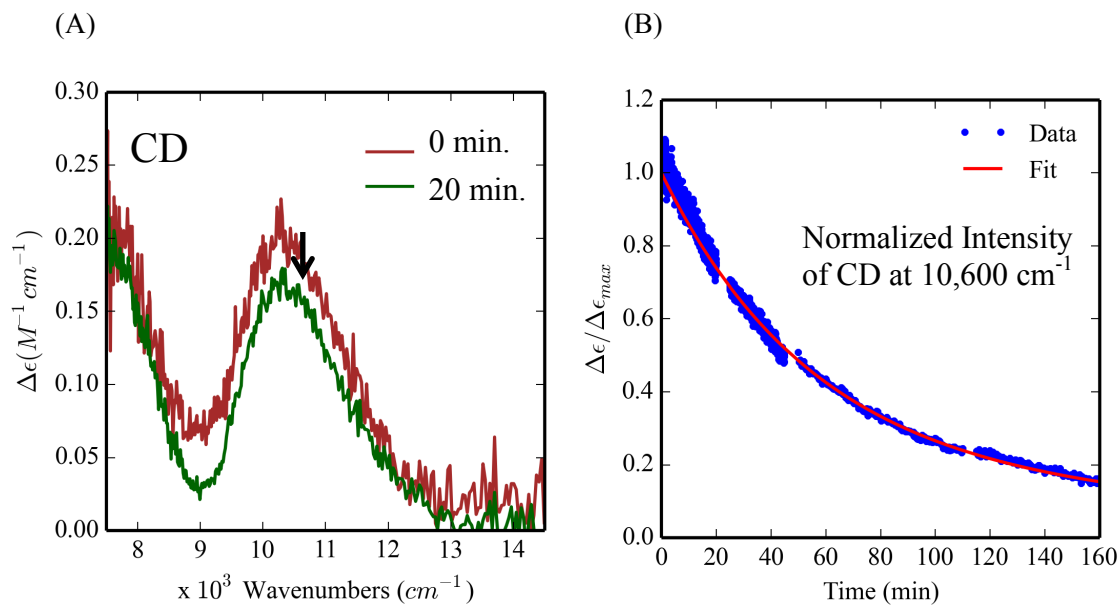


Figure 9: The biferrous CD features during the 4-aminophenol oxidation reaction for 3His-G4DFsc(Mut3). (A) CD of 3His-G4DFsc(Mut3)+4-AP before (red) and after (green) addition of O₂ saturated buffer. (B) The time course over 160 min of the normalized intensity of the CD feature at 10,600 cm^{-1} (red line is the kinetic fit). CD data collected at 4 °C in the presence of ~15-fold excess substrate (~0.25 mM protein).

1
2
3
4
5
6
7
8
9
10
11
12
13
14
15
16
17
18
19
20
21
22
23
24
25
26
27
28
29
30
31
32
33
34
35
36
37
38
39
40
41
42
43
44
45
46
47
48
49
50
51
52
53
54
55
56
57
58
59
60

CD spectroscopy was used to detect the amount of the biferrous form of the 3His variant present during 4-aminophenol oxidation under turnover conditions. After maintaining 90-100% intensity for ~10 min. (i.e. close to steady state) (Figure 9 (A) and Figure S10), there is a very slow decay of these NIR CD (the decay can be fit with 2 rates, $k_{d1} = 3 \times 10^{-4} \text{ s}^{-1}$ and $k_{d2} = 1.5 \times 10^{-5} \text{ s}^{-1}$, Figure 9 (B)). The decay may be correlated with the consumption of substrate and the oxidation of 3His-G4DFsc(Mut3) under substrate limited conditions. Given that the resting biferric form of the 3His does not show oxidase activity over 10 min (Figure 3 (G)) and the sustained presence of the biferrous form during turnover of 4-aminophenol oxidation, a 2-electron process may be invoked where O_2 is reduced by 2 electrons to H_2O_2 and 4-aminophenol is oxidized to quinone imine at the biferrous site. Any 2Fe(III) peroxy-intermediate during turnover should be rapidly reduced to the biferrous form. These data also suggest that 4-aminophenol inhibits the rebinding of the 3rd His residue to the biferrous site during steady state conditions. As substrate is depleted, the slow decay of the biferrous site (over ~ 2.7 hours, Figure 9 (B)) thus reflects rebinding of the 3rd His and oxidation of the 3His site to the minimally reactive 3His biferric species. Thus, after substrate binding, the 3His and 2His forms have similar active sites that are competent for 4-aminophenol oxidase reactivity where the bound substrate is oxidized and O_2 is reduced in a 2-electron process.

Oxygenase Activity.

Reactivity.

Our prior studies found that 3His-G4DFsc(Mut3), but not G4DFsc, was active in the oxygenation of *p*-anisidine. ⁵¹ This involved the oxidation of *p*-anisidine (P-AN, **5**) to the corresponding hydroxylamine (**6**). The hydroxylamine was directly observed when *p*-aminobenzonitrile was used as the substrate. However, in the case of the *p*-anisidine, the hydroxylamine product was instead oxidized to 4-nitroso-methoxybenzene (N-MB, **7**), which coupled with a second molecule of P-AN to form 4-methoxy-*N*-(4-nitrosophenyl)aniline (M-NPA, **8**) (Figure 10). The experimental conditions for these studies involved adding Fe(II) to a solution of apo-protein and substrate under aerobic conditions. While Fe(II) should be bound, these conditions allowed for either the biferric or biferrous forms of 3His-G4DFsc(Mut3) as the active species. This work extends on prior results to identify which form of 3His-G4DFsc(Mut3) is active.

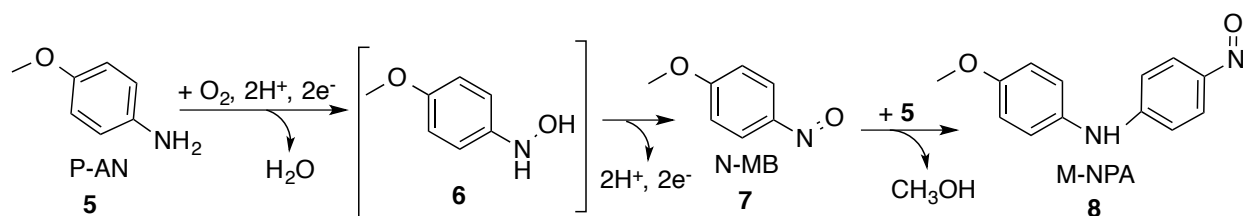


Figure 10: The reaction scheme of the oxidation of *p*-anisidine (P-AN) (**5**) to 4-hydroxylamine-methoxybenzene (**6**), with addition oxidation to 4-nitroso-methoxybenzene (N-MB) (**7**), and the coupling of N-MB and P-AN to form 4-methoxy-*N*-(4-nitrosophenyl)aniline (M-NPA) (**8**).

When *p*-anisidine substrate was incubated with biferrous 3His-G4DFsc(Mut3) anaerobically and then reacted with O_2 , the UV-Vis absorption spectra showed the production of

1
2
3 N-MB at 342 nm and the coupled product M-NPA at 431 nm (Figure 11 (A)). The UV-Vis
4
5 absorption spectra for a sample in which O₂ and *p*-anisidine were added simultaneously to
6
7 biferrous 3His-G4DFsc(Mut3) also showed reactivity but only ~1/2 that of the biferrous protein
8
9 with substrate preloaded (Figure 11 (B)). The biferric form of 3His-G4DFsc(Mut3) showed no
10
11 activity (Figure 11 (C)) provided the buffer was exchanged after the biferric state was formed
12
13 and prior to *p*-anisidine addition. [Note that without exchanging the buffer of the biferric protein,
14
15 *p*-anisidine oxidation was observed (Figure S11 (A)). However, this oxidation can be attributed
16
17 to the presence of hydrogen peroxide (where the protein has generated a stoichiometric amount),
18
19 which independently did test positively for *p*-anisidine oxidation (Figure S11 (B)) and showed
20
21 similar absorption changes (Figure S11 (C)) as exhibited by the biferric form if the buffer was
22
23 not exchanged.] These UV-Vis absorption results were confirmed by LCMS, where anaerobic
24
25 addition of *p*-anisidine to biferrous 3His-G4DFsc(Mut3) followed by addition of O₂ saturated
26
27 buffer (Figure S12 (A)) led to greater amounts of N-MB (m/z=138, retention time 12.6 min) and
28
29 product-NPA (m/z=229, retention time 24.21 min.) than the H₂O₂ present in the biferric reaction
30
31 mixture (Figure S12 (B)) (2 x the area of the peak associated with nitroso product and ~18 x the
32
33 area of the peak associated with the coupled product). These results show that substrate binding
34
35 to the biferrous 3His protein initiates the amino-oxygenation reaction.
36
37
38
39
40
41
42
43
44
45
46
47
48
49
50
51
52
53
54
55
56
57
58
59
60

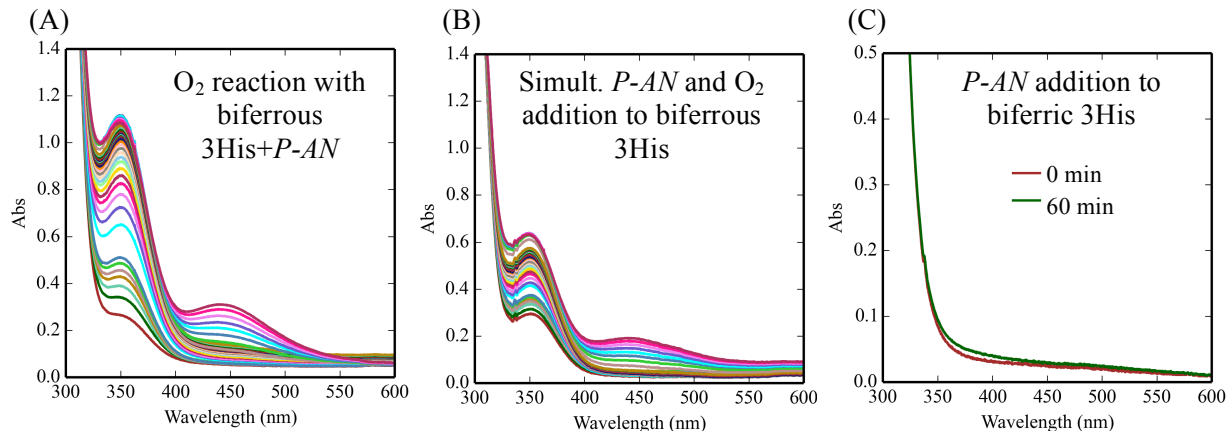


Figure 11: The oxidation of *p*-anisidine as followed by UV-Vis absorption spectroscopy. (A) *p*-anisidine was added anaerobically to biferrous 3His-G4DFsc(Mut3) followed by addition of O₂ saturated buffer. (B) *p*-anisidine and O₂ saturated buffer were added simultaneously to biferrous 3His-G4DFsc(Mut3). (C) *p*-anisidine was added to biferrous 3His-G4DFsc(Mut3) (buffer exchanged prior to *p*-anisidine addition to eliminate any presence of H₂O₂ in solution). (A) and (B) are data collected over 180 min. Data taken at 20 °C. Final samples contained 65 μM of protein and 1 mM of substrate.

Alternatively, for biferrous G4DFsc, the anaerobic addition of the *p*-anisidine substrate followed by O₂ saturated buffer led to no discernable peaks in the LCMS associated with product formation (Figure S12 (C)). The competition between substrate binding and O₂ reactivity can thus be excluded as a possible explanation for the lack of activity of the 2His form that was previously reported.⁵¹

Spectroscopic definition of substrate binding.

Since the reactivity studies indicate that substrate binding to the reduced 3His protein is necessary for amino-oxygenation reactivity, the effect of *p*-anisidine on the biferrous site was investigated with CD, MCD and VTVH MCD spectroscopy. Substrate addition (+P-AN) to G4DFsc and 3His-G4DFsc(Mut3) only minimally perturbs the CD (Figure 12 (A) and (B) top) and MCD (Figure 12 (A) and (B) bottom) spectra with slight shifts in the energies and intensities

of the bands. The most notable change is that the lower energy feature of the MCD spectrum of the 3His form shifts from $\sim 7,700\text{ cm}^{-1}$ (shoulder in red spectrum, Figure 12 (B) bottom) to $\sim 7,400\text{ cm}^{-1}$ (green spectrum in Figure 12 (B) bottom). These small changes indicate that the substrate binding affects the biferrrous site, but does not change the coordination, and thus, is not likely bound directly to the diiron center.

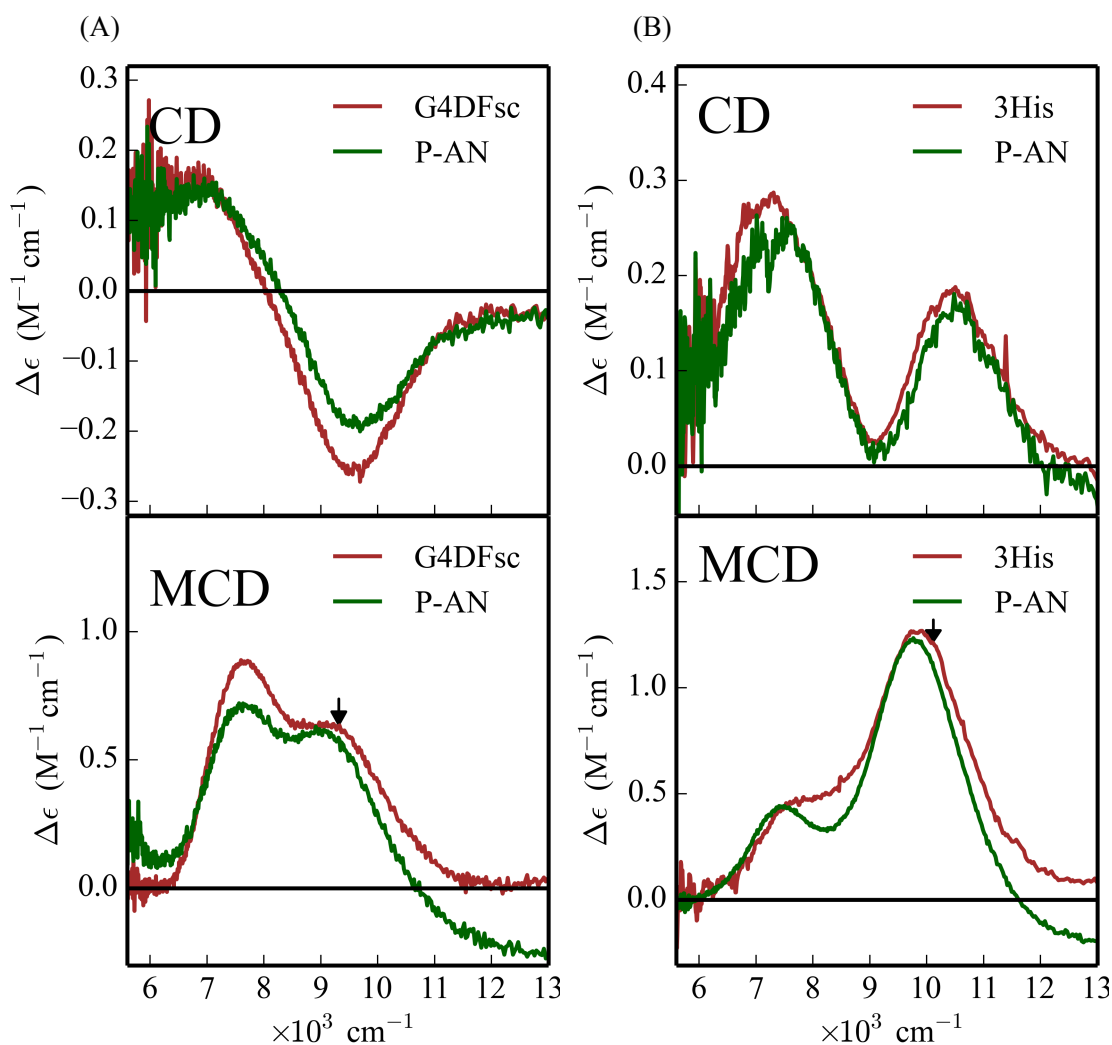


Figure 12: The effect of *p*-anisidine addition on the CD and MCD. The CD (top) and MCD (bottom) of (A) G4DFsc and (B) 3His-G4DFsc(Mut3) with unbound (red) and bound (green) forms. Protein concentration is $\sim 1\text{ mM}$ with 20-30 fold excess substrate. MCD data taken at 2 K and 7 T (baseline subtracted). CD data taken at 4 °C. Arrows in bottom spectra indicate where VTVH MCD data were taken.

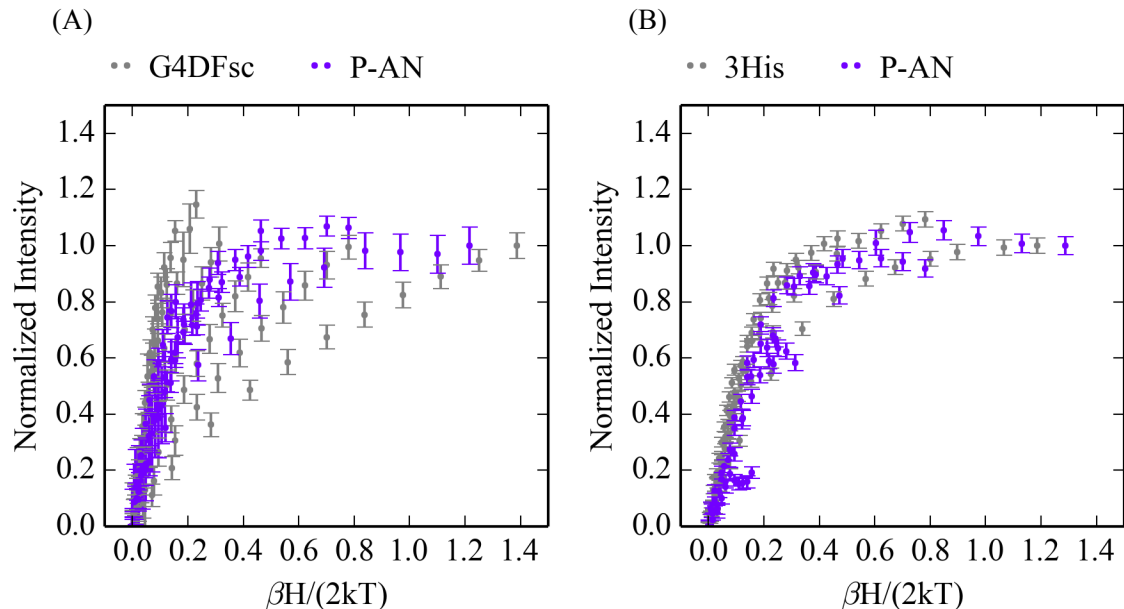


Figure 13: The effect of *p*-anisidine addition on the VTVH MCD isotherms. (A) The VTVH MCD of G4DFsc (grey) and G4DFsc+P-AN (purple) at $9,100\text{ cm}^{-1}$ is shown. (B) The VTVH MCD of 3His-G4DFsc(Mut3) (grey) and 3His-G4DFsc(Mut3)+P-AN (purple) at $10,400\text{ cm}^{-1}$ is shown. 2 K, 3 K, 5 K, 7.5 K, 10 K, 15 K, and 20 K isotherms are shown.

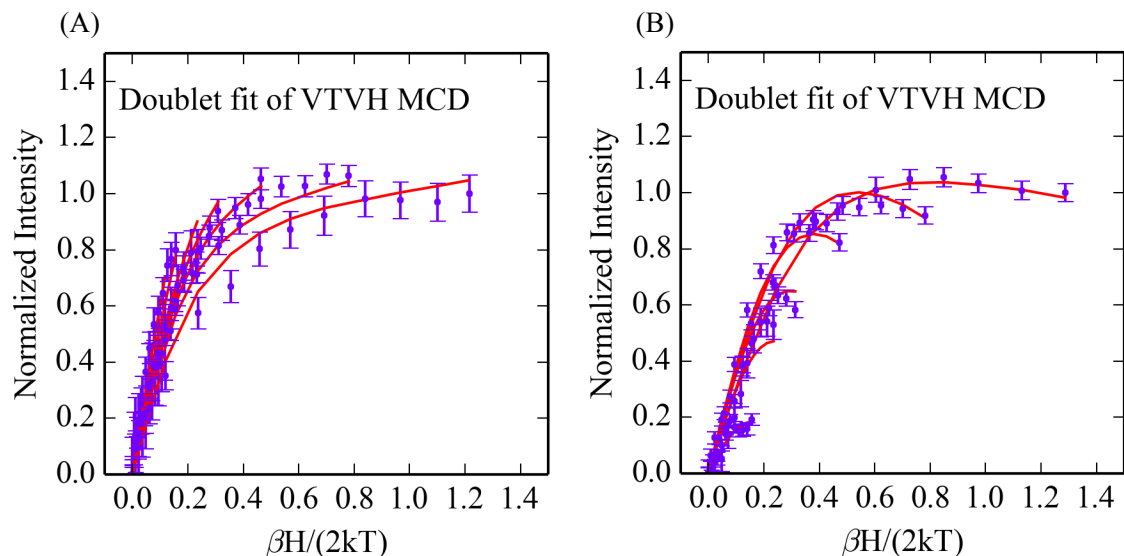


Figure 14: Doublet fits for the VTVH MCD data for (A) G4DFsc+P-AN and (B) 3His-G4DFsc(Mut3)+P-AN. Data for G4DFsc were collected at $9,100\text{ cm}^{-1}$ and those for the 3His form were collected at $10,500\text{ cm}^{-1}$.

Table 2: Spin Hamiltonian parameters for G4DFsc and 3His-G4DFsc(Mut3) in the presence of *p*-anisidine.

		G4DFsc	3His-G4DFsc(Mut3)
	$-J$ (cm ⁻¹)	< 2	$2-3$
Spin	D_1 (cm ⁻¹)	5-15	5-10
Hamiltonian	$(E/D)_1$	0.33	0.33
Parameters	D_2 (cm ⁻¹)	-5 to -15	-5 to -10
	$(E/D)_2$	0.33	0.33

While only slightly perturbing the CD and MCD features of both biferrous G4DFsc and 3His-G4DFsc(Mut3), *p*-anisidine addition does markedly change the VTVH MCD behavior for both forms (VTVH MCD curves change from grey to purple upon substrate binding in Figure 13 (A) and (B)). For G4DFsc+P-AN, the VTVH MCD data (Figure 14 (A)) were fit using the doublet model (*vide supra*) as described in Supporting Information. The VTVH MCD data of G4DFsc+P-AN indicate that $-J < 2$ cm⁻¹ (Table 2) for this form, which is less in magnitude than that found for G4DFsc without substrate ($-J \sim 3-4$ cm⁻¹). For 3His-G4DFsc(Mut3)+P-AN, doublet model fitting (see Supporting Information) of the VTVH MCD data (Figure 14 (B)) indicates that there is a slight increase in the magnitude of the antiferromagnetic coupling ($-J \sim 2-3$ cm⁻¹ 3His-G4DFsc(Mut3)+P-AN, and $1-2$ cm⁻¹ 3His-G4DFsc(Mut3)-P-AN) (Table 2).

The antiferromagnetic exchange coupling values for both G4DFsc+P-AN and 3His-G4DFsc+P-AN are consistent with μ -1,3 carboxylate bridges between the two Fe(II) sites. However, the change in their magnitude suggests that *p*-anisidine is binding near the biferrous site and perturbing the carboxylate bridges between the ferrous centers.

1
2
3 *Kinetics.*
4
5
6

7 Our previous studies of the O₂ reactivity of biferrous G4DFsc and 3His-G4DFsc(Mut3) suggest
8 that the exchange coupling and O₂ reaction rates are correlated, resulting from the O₂ reaction
9 occurring at only one Fe(II) site but being reduced by 2 electrons. The transfer of the 2nd electron
10 from the remote Fe(II) site would then occur through the carboxylate bridges. In this model, the
11 decrease in the carboxylate bridge mediated exchange coupling of G4DFsc upon addition of *p*-
12 anisidine would result in decreased O₂ reactivity. This is confirmed where the rate of the O₂
13 reaction for G4DFsc+P-AN is 0.002 s⁻¹ (Figure S14) (relative to 0.01-0.03 s⁻¹ without *p*-
14 anisidine).⁵² In contrast, the binding of *p*-anisidine to the 3His form results in only a small
15 change in exchange coupling (-J from 1-2 cm⁻¹ to 2-3 cm⁻¹) and the rate of obtaining steady state
16 for nitroso production (k ~ 0.045 s⁻¹, Figure S15) is close to the O₂ reaction rate of the 3His form
17 without substrate (0.01-0.06 s⁻¹).⁵²
18
19
20
21
22
23
24
25
26
27
28
29
30
31
32
33
34
35
36
37
38
39
40
41
42
43
44
45
46
47
48
49
50
51
52
53
54
55
56
57
58
59
60

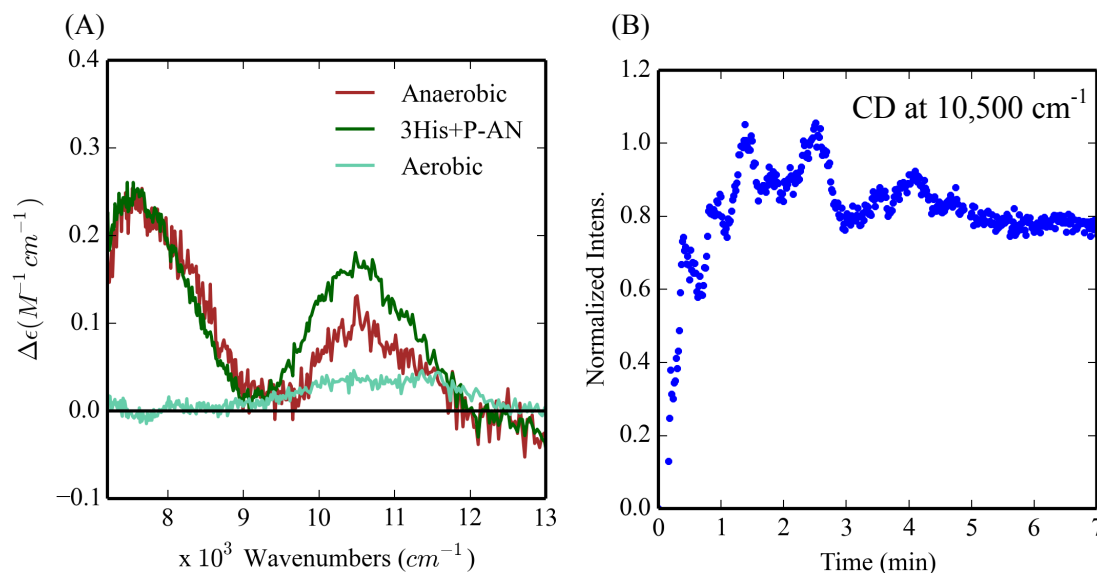


Figure 15: NIR CD spectra of the *p*-anisidine reaction with 3His-G4DFsc(Mut3). (A) CD spectra of the 3His protein in the presence of *p*-anisidine before exposure to O₂ (green), under aerobic conditions (teal), and 30 min after first allowing O₂ containing buffer (~250 μ M of O₂) to react for 60 sec and then sealing the CD cell to create a closed system. Protein concentrations for red and teal are 250 μ M. (B) The time dependence of the 10,500 cm^{-1} feature after first allowing 3His-G4DFsc(Mut3)+P-AN to react with O₂ followed by sealing the CD cell to create a closed system (see red in (A)). Data collected at 20 $^{\circ}$ C.

NIR CD and MCD spectroscopy were used to observe the biferrous bands of 3His-G4DFsc(Mut3) during the arylamine oxygenation reaction. Under aerobic conditions (i.e. turnover conditions), there are no NIR CD features present during production of the nitroso product (teal, Figure 15 (A)), which indicates that 3His-G4DFsc(Mut3) is mostly present in the biferric form at steady state, and thus, any reduction of the diiron center during turnover (Figure S16) must be rate limiting. In oxygen-depleted environments during nitroso production, the NIR CD and MCD features associated with biferrous 3His-G4DFsc(Mut3) are regenerated (Figure 15 (A, red) and (B) and Figure S17 (A)). Since *p*-anisidine does not reduce the biferric form of 3His-G4DFsc(Mut3) (Figure S17 (B)), the regeneration of Fe(II)Fe(II) state suggests that the biferric 3His form is reduced by a reaction intermediate during catalysis.

The oxygenation of *p*-anisidine to the nitroso product is a 4-electron process where the first 2-electron step should be the hydroxylation of the amine group followed by oxidation to the

1
2
3 nitroso product. The above results suggest that the biferrous 3His-G4DFsc(Mut3) variant
4
5 catalyzes the oxygenation of the amine group to a hydroxylamine and results in a biferric
6
7 species. This hydroxylamine may then be oxidized to the nitroso product by the Fe(III)Fe(III)
8
9 state of the 3His protein, regenerating the Fe(II)Fe(II) state in the rate limiting step.
10
11
12
13

14 15 **Discussion**

16
17 Our previous studies identified markedly different reactivities in the 2His and 3His 4A→4G
18
19 variants of DFsc, where 4-aminophenol oxidase activity was observed in the 2His variant
20
21 (G4DFsc), but not in the 3His variant (3His-G4DFsc(Mut3)), and arylamine oxygenase activity
22
23 was detected for the 3His variant, but not the 2His form.⁵¹ This study has extended these results
24
25 to understand the molecular basis for these reactivity differences.
26
27

28
29 *Oxidase.* By systematically controlling the reaction conditions, we have identified the active
30
31 species for the 4-aminophenol oxidation. Both the 2His and 3His variants display oxidase
32
33 activity when substrate binding to the biferrous site preceded the reaction with O₂. The CD,
34
35 MCD and VTVH MCD studies show substantial perturbation of the biferrous sites of both
36
37 G4DFsc and 3His-G4DFsc(Mut3) by 4-aminophenol. While 4-aminophenol addition to G4DFsc
38
39 resulted in a new higher energy feature (~10,500 cm⁻¹) in the MCD spectrum, its addition to
40
41 3His-G4DFsc(Mut3) causes a marked increase in MCD intensity ($\Delta\epsilon \sim 1$ to ~ 7 cm⁻¹M⁻¹). These
42
43 perturbations suggest that this substrate binds directly to the biferrous sites of both forms.
44
45
46
47

48
49 Gaussian resolution of the CD and MCD features for both G4DFsc and 3His-
50
51 G4DFsc(Mut3) in the presence of 4-AP reveal three bands that are similar in sign and energy to
52
53 3His-G4DFsc(Mut3) without 4-AP and suggest that all three forms have a 5-coordinate+6-
54
55 coordinate trigonal bipyramidal biferrous site. Given the lack of increased coordination in the
56
57
58
59
60

1
2
3 3His form upon substrate addition, it may be inferred that structural limitations prevent the
4 substrate from simply binding to the open site on the 5-coordinate iron center of the 3His variant.
5
6

7
8 The VTVH MCD data of biferrous G4DFsc and 3His-G4DFsc(Mut3) were also
9 perturbed by the binding of 4-aminophenol. The associated spin-Hamiltonian parameters show
10 that both forms are weakly antiferromagnetic coupled, indicating they still have μ -1,3
11 carboxylates bridging the biferrous site. These spectral data show that G4DFsc+4-AP and 3His-
12 G4DFsc(Mut3)+4-AP have similar site structures where 4-aminophenol binds to and increases
13 the coordination of one Fe(II) in G4DFsc while replacing a ligand (likely the additional His) in
14 3His-G4DFsc(Mut3).
15
16
17
18
19
20
21
22
23

24
25 Substrate binding to the biferrous site initiates the oxidase activity. Therefore, the kinetics
26 of 4-aminophenol binding to the biferrous sites of G4DFsc and 3His-G4DFsc(Mut3) were
27 explored with "freeze quench" MCD spectroscopy. The binding rate of 4-aminophenol for
28 G4DFsc ($k_B = 0.027\text{-}0.042\text{ s}^{-1}$) was found to be an order of magnitude greater than that for the
29 3His variant ($k_B = 0.003\text{-}0.0046\text{ s}^{-1}$). However, the O_2 reaction rates of both proteins are
30 comparable at around $\sim 10^{-2}\text{ s}^{-1}$.⁵² Based on the kinetics, 4-aminophenol binding to the 3His
31 variant is an order of magnitude less than the O_2 reaction rate. Thus, when substrate and O_2 are
32 simultaneously added, the biferrous 3His form first reacts with O_2 to generate an inactive biferric
33 species prior to substrate binding, which renders the protein ineffective for substrate oxidation.
34 Since the 2His form exhibits faster 4-aminophenol binding (likely due to the decreased
35 coordination of the biferrous site), the slow substrate binding in the 3His variant may be
36 attributed to its competition with the additional His ligand. The 3His-G4DFsc(Mut3) variant
37 therefore becomes active only upon anaerobic incubation of substrate with the biferrous form,
38 presumably following replacement of the additional His ligand at the active site by 4-AP.
39
40
41
42
43
44
45
46
47
48
49
50
51
52
53
54
55
56
57
58
59
60

1
2
3
4 NIR CD spectroscopy was used to monitor the ferrous $d \rightarrow d$ transitions during 4-
5
6 aminophenol oxidation and showed the dominant presence of the biferrous 3His-G4DFsc(Mut3)
7
8 species during steady state. Given that the resting biferric forms were inactive for substrate
9
10 oxidation, a 2-electron process may be invoked where O_2 is reduced to H_2O_2 (which is lost) and
11
12 4-aminophenol is oxidized to the benzoquinone imine at the biferrous site (Figure 16). The
13
14 presence of 4-aminophenol likely inhibits rebinding of the 3rd His ligand to the biferrous site
15
16 during turnover. There are several possible mechanisms for inhibition of the rebinding of the 3rd
17
18 His: 1) one 4-aminophenol molecule stays bound during turnover, or 2) the 4-aminophenol out-
19
20 competes the 3rd His protein residue in binding to the diiron center. The former possibility
21
22 would involve a ping-pong mechanism since only one open coordination site is available for O_2
23
24 reduction and 4-aminophenol oxidation, while the latter would allow for direct O_2 reduction at
25
26 one iron site and 4-aminophenol oxidation at the other.
27
28
29
30
31

32 The observed lack of oxidase activity of the biferric species in G4DFsc and 3His-
33
34 G4DFsc(Mut3) is in contrast to other DF constructs.⁵³ Since the NIR CD and MCD data
35
36 demonstrate that substrate is accessible to the diiron sites, the lack of activity may be related to
37
38 either unfavorable thermodynamics (redox potentials of G4DFsc and 3His-G4DFsc(Mut3) are
39
40 unknown, but the 2-electron potential for 4-aminophenol is ~ 300 mV (converted to SHE, pH 7-
41
42 9))^{54,55} or the coordinative saturation that is proposed for the ferric centers in G4DFsc and 3His-
43
44 G4DFsc(Mut3).⁵²
45
46
47
48
49
50
51
52
53
54
55
56
57
58
59
60

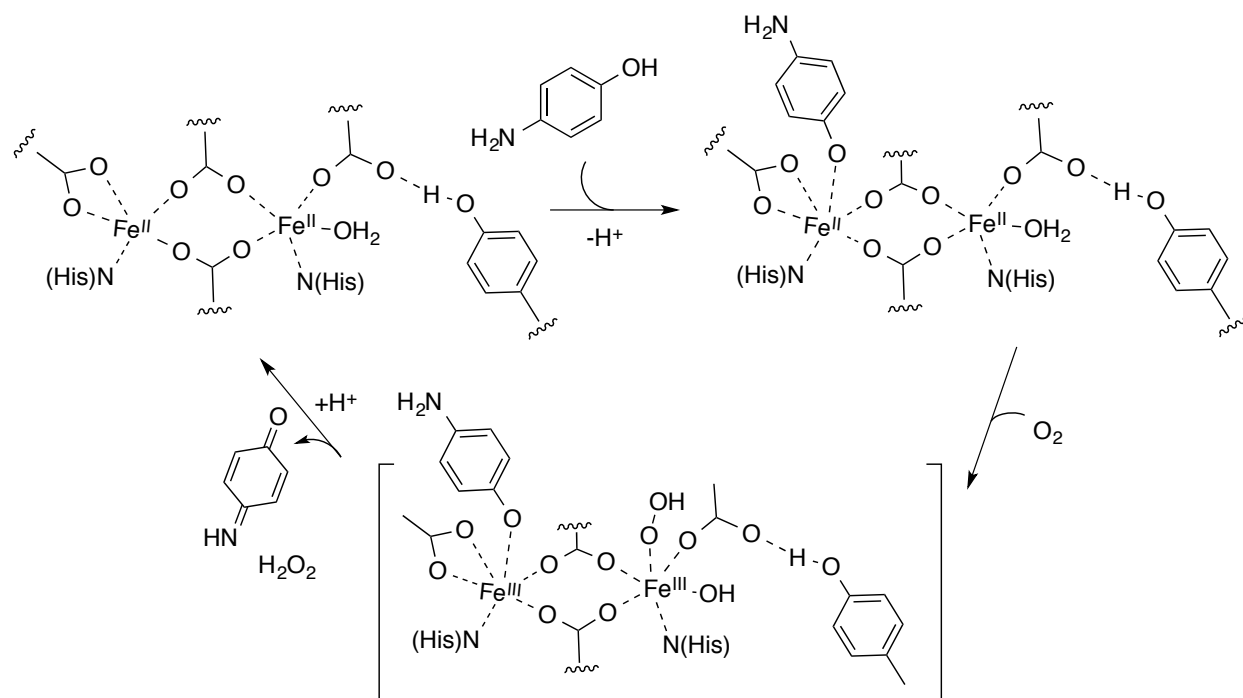


Figure 16: Mechanistic scheme of 4-aminophenol oxidation with biferrous protein.

Oxygenase. The oxygenation of *p*-anisidine to 4-nitroso-methoxybenzene (N-MB) by the 4A→4G DF variants observed in prior studies⁵¹ was further explored to understand the differential reactivity between G4DFsc and 3His-G4DFsc(Mut3) as well as to identify the catalytically relevant species. In particular, the effects of anaerobic *p*-anisidine addition to the biferrous site of both G4DFsc and 3His-G4DFsc(Mut3) were spectroscopically studied to correlate geometric perturbations with reactivity.

Similar to prior results, these studies confirm that G4DFsc lacks oxygenase activity even with anaerobic addition of *p*-anisidine to the biferrous form. The NIR CD and MCD spectra show slight shifts in energies and intensities for the features associated with Fe(II) $d \rightarrow d$ transitions upon substrate binding to biferrous G4DFsc. These minimal spectral changes suggest that while the substrate does not bind directly to the biferrous site, it does bind near enough to

1
2
3 perturb the biferrous site geometry. The VTVH MCD data of G4DFsc+P-AN indicate a decrease
4
5 in antiferromagnetic coupling. Our prior results on the O₂ reactivity of these DF variants indicate
6
7 that O₂ reduction occurs at a single iron center,⁵² thus, the rate of the 2-electron reduction of O₂
8
9 may be influenced by the exchange coupling of the two Fe(II) sites due to μ -1,3 carboxylate
10
11 bridges. The decrease in anti-ferromagnetic coupling in G4DFsc upon P-AN addition may thus
12
13 slow the rate of O₂ reduction. However, the lack of oxygenase reactivity likely reflects an
14
15 improper orientation of the substrate in relation to the reactive hydroperoxy species that would
16
17 be produced upon O₂ reduction (*vide infra*).
18
19
20
21

22 For 3His-G4DFsc(Mut3), substrate binding to the reduced protein was determined to be
23
24 important for oxygenase activity. Similar to G4DFsc, the NIR CD and MCD spectra of the 3His
25
26 form show only slight energy shifts and intensity changes for the Fe(II) d \rightarrow d transitions upon
27
28 the addition of *p*-anisidine, which thus indicates that substrate binds near (but not directly to) the
29
30 biferrous site. In contrast to G4DFsc, substrate addition to 3His-G4DFsc(Mut3) slightly
31
32 increases the antiferromagnetic coupling, which would not slow the rate of O₂ reduction at a
33
34 single iron center. These results highlight a differential perturbation of the *p*-anisidine substrate
35
36 on the biferrous centers of G4DFsc and 3His-G4DFsc(Mut3) that may influence oxygen
37
38 dependent reactivities.
39
40
41
42

43 The oxygenation of *p*-anisidine to the nitroso product N-MB is a 4-electron process,
44
45 requiring a 2-electron exogenous reductant for single turnover in the proposed mechanisms of
46
47 AurF.^{20,29} Interestingly, the catalytic turnover of N-MB is detected in the 3His-G4DFsc(Mut3)
48
49 system without the addition of exogenous reducing equivalents. The appearance of Fe(II) d \rightarrow d
50
51 transitions of 3His-G4DFsc(Mut3) during *p*-anisidine oxygenation upon O₂ depletion indicates
52
53 that the Fe(II)Fe(II) state is regenerated during turnover. These observations are consistent with
54
55
56
57
58
59
60

the formation of an initial 2-electron oxidized hydroxylamine product that subsequently reduces the biferric state to regenerate the biferrous site and form the 4-nitroso-methoxybenzene product. A lack of Fe(II) $d \rightarrow d$ transitions during steady state suggests that this reduction of the biferric site by the hydroxylamine intermediate would be the slow step in turnover.

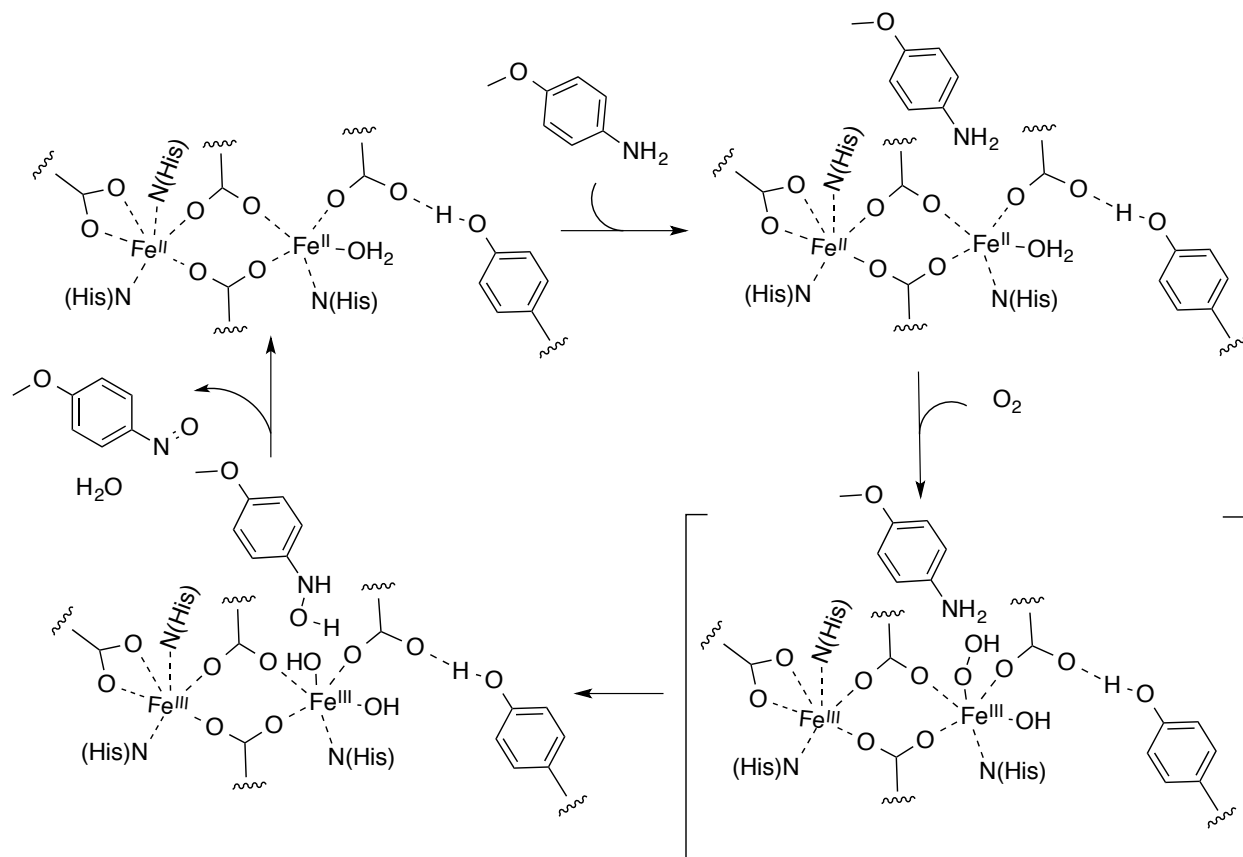


Figure 17: Mechanistic scheme for oxygenation of *p*-anisidine by 3His-G4DFsc(Mut3)

Based on the above results, a mechanism for the oxygenation of *p*-anisidine by 3His-G4DFsc(Mut3) is proposed in Figure 17. First, *p*-anisidine binds near the biferrous site (perhaps through hydrogen-bonding interactions between the amine group of *p*-anisidine and a residue near the active site). This is followed by O₂ end-on binding to the unsaturated Fe(II) site, leading to its reduction by 2-electrons to generate a hydroperoxy biferric species. Then, hydroxylation of

1
2
3 the amine group of *p*-anisidine is likely to proceed via an electrophilic attack on the nitrogen lone
4 pair by the hydroperoxy species. This hypothesis is consistent with studies of amine
5 hydroxylation catalyzed by AurF, where protonation of the bridged peroxy species was found to
6 drive this electrophilic attack.⁵⁶ However, in the case of AurF, the hydroperoxy species is
7 bridged rather than end-on. In our case, the 3rd His saturates one iron center, preventing bridging
8 of the peroxide, but still allowing for protonation and electrophilic attack. The biferric species
9 formed upon substrate oxygenation would then be reduced by the resultant hydroxylamine,
10 forming the nitroso product and regenerating the biferrous site for turnover.
11
12

13 *Conclusions.* These studies on *de novo* designed proteins offer molecular level insight into the O₂
14 dependent chemistry of binuclear non-heme iron enzymes. Contrary to our prior results, 3His-
15 G4DFsc(Mut3) does equivalent oxidase reactivity to that of the 2His form, provided enough time
16 is given for substrate binding. This activates the 3His-G4DFsc(Mut3) through substitution of a
17 ligand. The results illustrate that protein design may be used to inhibit oxidase reactivity by
18 altering the substrate-binding rate through saturating the coordination of an iron site. While
19 G4DFsc lacks arylamine oxygenase activity, *p*-anisidine still binds near the diiron sites in both
20 3His-G4DFsc(Mut3) and G4DFsc. However, there is a differential perturbation that may reflect
21 reactivity differences. Saturating one Fe(II) of the biferrous site but enabling 2-electron transfer
22 through μ -1,3 carboxylate bridges appears to facilitate the formation of an end-on hydroperoxy
23 species at one Fe center that is competent in electrophilic attack on the lone pair of the amine
24 group. In contrast to some mechanisms proposed for AurF,^{20,29} 3His-G4DFsc(Mut3) appears to
25 be a mixed function oxidase where it performs both oxygenation and oxidation of the *p*-anisidine
26 substrate. The apparent necessity of direct substrate binding to the diiron site suggests the
27 importance of a sufficient electron transfer pathway in oxidase reactivity, while the presence of
28
29
30
31
32
33
34
35
36
37
38
39
40
41
42
43
44
45
46
47
48
49
50
51
52
53
54
55
56
57
58
59
60

1
2
3 substrate in a protein-binding pocket may facilitate oxygenase reactivity. These studies
4
5 demonstrate how modification of substrate binding through additional protein ligation may tune
6
7
8 the function of the active site in binuclear non-heme iron enzymes.
9
10
11
12
13
14
15
16
17
18
19
20
21
22
23
24
25
26
27
28
29
30
31
32
33
34
35
36
37
38
39
40
41
42
43
44
45
46
47
48
49
50
51
52
53
54
55
56
57
58
59
60

Materials and Methods

Preparation of Apo-Protein.

Apo-protein of G4DFsc and 3His-G4DFsc(Mut3) were prepared as previously described.⁵¹

Preparation of Biferrous Protein.

Biferrous protein of G4DFsc and 3His-G4DFsc(Mut3) were prepared anaerobically as previously described.⁵² This preparation included degassing apo-protein on a Schlenk line by gentle pump/purge cycles followed by purging the headspace for continuously for several hours. Protein was then transferred to a glove box and loaded with Fe(II) (FeSO₄·6H₂O from J.T. Baker) by adding ~1.7-1.8 equivalents of ferrous ammonium sulfate (solution prepared anaerobically) and allowing the solution to incubate for ~15-20 min. For the buffer, MOPS and NaCl were obtained from Sigma-Aldrich.

Oxidase Activity Assays.

For substrate preloaded samples, 4-aminophenol (in 30% DMF prepared anaerobically) was anaerobically added to biferrous protein (G4DFsc or 3His-G4DFsc(Mut3) in 150 mM MOPS/150 mM NaCl at pH 7) and incubated for 20 min. *m*-phenylenediamine was then added to the protein sample before being loaded into an anaerobic cell for absorption experiments. An equivalent volume of O₂ saturated buffer (sparging buffer with O₂ gas in a closed vessel at 4 °C for 15 min) was added to the sample (resulting in dilution of protein by 1/2) and rapidly mixed

1
2
3 immediately before collecting data. For simultaneous addition of O₂ saturated buffer and 4-
4 aminophenol to the protein, 4-aminophenol and *m*-phenylenediamine solutions were prepared in
5 the glove box prior to mixing experiments. Biferrous protein was loaded into an anaerobic cell
6 (in a glove box). Immediately before addition to the protein sample, 4-aminophenol and *m*-
7 phenylenediamine were added to the O₂ saturated buffer, which was then added to the biferrous
8 protein and the UV-Vis absorption spectra were collected after a few seconds of rapid mixing.
9
10 Resting G4DFsc (Species C) and 3His-G4DFsc(Mut3) biferric forms were prepared by adding
11 O₂ saturated buffer (equivalent volume, dilution of protein by one-half), allowing the reaction to
12 proceed for at least two hours at 4 °C. This sample was then added to a UV-Vis absorption cell.
13
14 4-aminophenol and *m*-phenylenediamine were added and mixed immediately before initiating
15 data collection. For biferric Species B of G4DFsc, biferrous protein was prepared followed by O₂
16 saturated buffer addition, which was allowed to react for ~100 sec (~50-70% species B). 4-
17 aminophenol and *m*-phenylenediamine were then added to the sample and data were collected.
18
19 Final concentrations (after O₂ saturated buffer addition) of protein, 4-aminophenol and *m*-
20 phenylenediamine were 10 μM for protein, 3.9 mM 4-aminophenol, and 10 mM *m*-
21 phenylenediamine. The concentrations of DMF in the protein solutions were kept below 3%. In
22 all experiments, after addition of O₂ saturated buffer, the samples were held under aerobic
23 conditions. A circulator connected to the UV-Vis cell holder was used to maintain the absorption
24 cell at 4-12 °C.
25
26
27
28
29
30
31
32
33
34
35
36
37
38
39
40
41
42
43
44
45
46
47
48
49
50

51 *NIR CD and MCD of 4-aminophenol addition to biferrous protein*

52
53

54 For the CD experiments, biferrous protein was prepared in the glove box. 4-aminophenol was
55 added (in ~15 fold excess) to biferrous protein (~1-2 mM) and the protein sample was incubated
56
57
58
59
60

1
2
3 for ~20 min. The sample was then loaded into an anaerobic CD cell and data measurements were
4 collected. A circulator connected to the CD cell holder was used to maintain the anaerobic quartz
5 CD cell at 4-12 °C. Multiple scans (5-20) were averaged. The CD spectrum of apo-protein was
6 subtracted from the spectra. For MCD experiments, protein samples were prepared with 4-
7 aminophenol (~1 mM in protein incubated for ~20 min. with ~15 fold excess 4-aminophenol and
8 in 54% d-glycerol (d8-glycerol; 98% 2H from Cambridge Isotope Laboratories) and 46% buffer
9 (150 mM MOPS/150 mM NaCl in D₂O (D₂O; 99.9% 2H) at pD 7). These samples were loaded
10 into MCD cells under anaerobic conditions and immersed into liquid nitrogen prior to data
11 collection. CD and MCD spectra were fit with the minimum number of Gaussian peaks required
12 for the data using a non-linear least-squares procedure that allows for variation in peak width and
13 energy positions between the CD and MCD fits. For the time dependent MCD experiments, a
14 solution of 4-aminophenol in 54% deuterated glycerol was anaerobically prepared. 4-
15 aminophenol solution (in d-glycerol) was injected into an MCD cell with biferrous protein (in
16 54% d-glycerol and 46% deuterated buffer) in an anaerobic environment, quickly mixed, and
17 incubated for different time intervals (e.g. 0.5 min, 5 min, etc.) prior to being immersed into
18 liquid nitrogen. MCD spectra shown are the averages of 5-20 scans. The averaged spectra taken
19 at the same magnitude but oppositely signed fields were averaged (e.g. $((+7T)-(-7T))/2$) as well
20 to subtract out the baseline. Both the near IR (600-1900 nm region) CD and MCD data were
21 collected on a JASCO J730D spectropolarimeter with a cooled InSb detector. The concentrations
22 of DMF in the protein samples were kept below 3%. Deuterium oxide and d-glycerol were
23 obtained from Cambridge Isotope Laboratories (Andover, MA).
24
25
26
27
28
29
30
31
32
33
34
35
36
37
38
39
40
41
42
43
44
45
46
47
48
49
50
51

52
53
54
55 *CD kinetics of 4-aminophenol oxidation.*
56
57
58
59
60

1
2
3
4
5
6 A solution of 4-aminophenol and biferrous protein was prepared (0.5 mM of protein with ~15
7
8 fold excess of 4-aminophenol in regular H₂O buffer) anaerobically where the sample was
9
10 incubated for ~20 min before being placed into an anaerobic quartz CD cell. O₂ saturated buffer
11
12 was prepared by sparging the buffer with O₂ gas in a sealed container for ~15 min at 4 °C. A
13
14 circulator connected to the CD cell holder was used to maintain temperature at 4-12 °C. Prior to
15
16 O₂ saturated buffer addition, the CD spectrum of the biferrous protein with 4-aminophenol was
17
18 measured. The JASCO J730D spectropolarimeter was fixed at 10,600 cm⁻¹. The CD intensity at
19
20 the associated time points were collected upon O₂ saturated buffer addition (where the protein
21
22 sample was diluted by 1/2). A complete CD spectrum was again taken after ~20 min, 1 hour, and
23
24 ~6 hours. A cooled InSb detector was used for data collection. The concentrations of DMF in the
25
26 protein samples were kept below 3%. After O₂ saturated buffer addition, samples were kept
27
28 under aerobic conditions.
29
30
31
32
33

34 35 36 *Oxygenase Activity Assays.* 37 38

39
40
41 For substrate bound protein experiments, *p*-anisidine was anaerobically added to biferrous
42
43 protein and incubated for ~20 min. The sample was then placed in an anaerobic UV-Vis
44
45 absorption cell. O₂ saturated buffer was added to the protein solution (dilution of protein by 1/2)
46
47 at 20 °C, rapidly mixed with a pipet and spectral collection as initiated. Scans were measured
48
49 every 10 seconds for the first minute, every minute for the first 10 min, and then every 10
50
51 minutes afterward. After addition of O₂ saturated buffer (prepared by sparging O₂ gas into buffer
52
53 in a closed vessel for ~15 min. at 20 °C), the sample was maintained under aerobic conditions.
54
55
56
57
58
59
60

1
2
3 For simultaneous addition of substrate and O₂ to the protein, biferrous protein was prepared
4 anaerobically and placed into an anaerobic UV-Vis absorption cell. Substrate was added to O₂
5 saturated buffer, which was then added to the protein solution (dilution of protein by 1/2) in the
6 UV-Vis absorption cell immediately before data collection. Absorption spectra were
7 collected every 10 seconds for the first minute, every minute for the first 10 minutes, and then
8 every 10 minutes. For *p*-anisidine addition to the biferric form, the biferric species was formed
9 by addition of O₂ saturated buffer to biferrous protein and allowed to react for 1-2 hours. The
10 sample was then buffer exchanged to remove any H₂O₂ produced during the reaction. This
11 sample was then loaded into a UV-Vis absorption cell, and a single UV-Vis absorption spectrum
12 was collected. *p*-anisidine was then added to the protein sample and UV-Vis absorption spectra
13 were collected every 10 seconds for the first minute, every minute for the first 10 minutes, and
14 then every 10 minutes. Final samples contained 65 μM of protein and 1 mM of substrate in 150
15 mM MOPS/150 mM NaCl buffer at pH 7.
16
17
18
19
20
21
22
23
24
25
26
27
28
29
30
31
32
33

34 For the experimental details concerning the LCMS of product formation, the H₂O₂ and
35 non-buffer exchanged biferric species controls of *p*-anisidine oxidase assays, and UV-Vis
36 absorption monitoring of the O₂ reactivity of biferrous G4DFsc in the presence of *p*-anisidine,
37 see the methods section in supporting information.
38
39
40
41
42
43
44
45

46 *NIR CD and MCD of p-anisidine addition to biferrous protein.*

47
48
49
50

51 For CD experiments, *p*-anisidine was anaerobically added to biferrous protein (in D₂O buffer)
52 and allowed to incubate for ~20 min. The sample (~1-2 mM protein and 20-30 fold excess
53 substrate) was then placed into an anaerobic CD cell. Multiple scans (5-20) of the spectrum were
54
55
56
57
58
59
60

1
2
3 collected on a JASCO J730D spectropolarimeter with a cooled InSb detector and averaged. The
4
5 CD of apo-protein was subtracted from these data. MCD cells were prepared by mixing d-
6
7 glycerol with substrate-loaded biferrous protein CD samples (54% glycerol, 46% buffer/protein
8
9 solution) and injecting the sample into the MCD cells under anaerobic conditions. The samples
10
11 were then immersed into liquid nitrogen. Multiple scans (5-20) were taken and averaged at
12
13 varying fields (± 7 T, ± 5 T, ± 3 T, ± 1 T, and 0 T) and temperatures (2 K, 5 K, 10 K, 20 K). The
14
15 baseline of the MCD data was subtracted by averaging positive and negative fields (e.g. $((+7T)-$
16
17 $(-7T))/2$).

21
22
23
24
25 *CD kinetics of p-anisidine oxygenation.*

26
27
28
29 Substrate (*p*-anisidine) was added to biferrous protein prepared anaerobically (in ~30 fold
30
31 excess) and allowed to incubate for ~20 min. The protein sample (~0.5 mM protein in H₂O
32
33 buffer) was then loaded into the anaerobic CD cell. For steady state conditions, O₂ saturated
34
35 buffer was added to the sample (dilution of protein by 1/2), the CD features were monitored at
36
37 10,600 cm⁻¹ for 60 min and a CD spectrum was collected under aerobic conditions after 1 hour
38
39 (taking ~5 scans and averaging them). This sample was then degassed, concentrated to ~1/2
40
41 volume and mixed with d-glycerol (54 % v/v). The sample was then injected into an MCD
42
43 sample cell under anaerobic conditions and immersed into liquid nitrogen. Multiple scans were
44
45 taken of the MCD spectrum at 2 K and ± 7 T and averaged. The MCD spectra at positive and
46
47 negative fields were averaged to subtract baseline. For monitoring of the reaction under non-
48
49 steady state conditions by CD spectroscopy, a substrate-bound biferrous protein sample was
50
51 prepared (~30 fold excess substrate, 0.5 mM protein) as above. The protein sample was added to
52
53
54
55
56
57
58
59
60

1
2
3 an anaerobic CD cell and the CD spectrum was collected. The CD intensity at $10,600\text{ cm}^{-1}$ was
4
5 monitored for ~ 60 s as an equal volume of O_2 containing buffer ($\sim 250\text{ }\mu\text{M}$) was mixed with the
6
7 protein solution under aerobic conditions. Then, the CD cell was sealed and the CD intensity at
8
9 $10,600\text{ cm}^{-1}$ was monitored for an additional 30 minutes. Upon completion, multiple scans of the
10
11 CD spectrum were taken and averaged. The CD spectrum of apo-protein was subtracted.
12
13
14
15
16

17
18 *Near IR VTVH MCD Experiments.*
19

20
21 100-200 scans of the MCD intensity at specific energies were collected for temperatures of 2, 3,
22
23 5, 7.5, 10, 15, 20, and 25 K at fields of 0, ± 0.35 , ± 0.7 , ± 1.4 , ± 2.1 , ± 2.8 , ± 3.5 , ± 4.2 , ± 4.7 , ± 5.6 ,
24
25 ± 6.3 , and ± 7.0 T. These measurements were averaged for each field at each temperature. The
26
27 reported data are averages of baseline-subtracted measurements for positive and negative field
28
29 taken at the same temperature (error bars represent the propagation of errors from the standard
30
31 deviations). The chi-squared value was used to judge the goodness of fit for the VTVH MCD
32
33 data. The VTVH MCD data were fit using doublet models as described previously.⁶
34
35
36
37
38
39
40
41
42
43
44
45
46
47
48
49
50
51
52
53
54
55
56
57
58
59
60

Acknowledgments

This work was supported by the NSF (MCB-0919027 to E.I.S. and CHE-1413295 to W.F.D.) and the NIH (F32-GM808852 and R15-GM110657 to A.J.R. and GM54616 and GM71628 to W.F.D.). We thank the Vincent Coates Foundation Mass Spectrometry Laboratory (Stanford University Mass Spectrometry), particularly Ludmila Alexandrova, for acquisition of the LCMS data included in the Supporting Information.

Supporting Information Available

UV-Vis absorption spectra of 4-aminophenol oxidation with 3His-G4DFsc(Mut3) without *m*-phenylenediamine; UV-Vis absorption of 4-aminophenol oxidation in the presence of *m*-phenylenediamine without protein; CD spectra of G4DFsc and 3His-G4DFsc(Mut3) with and without 4-aminophenol addition; MCD spectra of G4DFsc+4-AP at different temperatures and magnetic fields showing C-term behavior; Doublet fitting of the VTVH MCD data for G4DFsc+4-AP and 3His-G4DFsc(Mut3)+4-AP; Composite MCD spectrum for 0.6xG4DFsc+4-AP and 0.4xG4DFsc; MCD spectra of 4-aminophenol addition to 3His-G4DFsc(Mut3) at different times; Composite MCD spectrum of 0.68x3His-G4DFsc(Mut3)+4-AP and 0.32x3His-G4DFsc(Mut3); Kinetic trace for the 470 nm feature of 3His-G4DFsc(Mut3)+4-AP reacted with O₂ saturated buffer; UV-Vis absorption spectrum of *p*-anisidine oxidation by H₂O₂ and non-buffer exchanged biferric 3His-G4DFsc(Mut3); LCMS data for O₂ reaction with biferric and biferrous 3His-G4DFsc(Mut3)+P-AN and biferrous G4DFsc+P-AN; MCD spectra at different temperatures for 3His-G4DFsc(Mut3)+P-AN; Doublet fitting of the VTVH MCD data for G4DFsc+P-AN and 3His-G4DFsc(Mut3)+P-AN; UV-Vis absorption spectra of O₂ reaction with G4DFsc+P-AN; Pre-steady state kinetic traces (near IR CD and UV-Vis absorption) for O₂ reaction with 3His-G4DFsc(Mut3)+P-AN; UV-Vis absorption after 48 hours of O₂ reaction with 3His-G4DFsc(Mut3)+P-AN; MCD of O₂ depleted 3His-G4DFsc(Mut3)+P-AN samples; Correlation energy diagram for G4DFsc+P-AN and 3His-G4DFsc(Mut3)+P-AN; Materials and Methods for LCMS of product formation, H₂O₂+P-AN and non-buffer exchanged biferric 3His-G4DFsc(Mut3)+P-AN controls, and UV-Vis absorption spectra of the O₂ reaction with G4DFsc+P-AN. This material is available free of charge via the Internet at <http://pubs.acs.org>.

References

1. Fishman, A.; Tao, Y.; Bentley, W. E.; Wood, T. K. *Biotechnol. Bioeng.* **2004**, *87*, 779-790.
2. Schirmer, A.; Rude, M. A.; Li, X.; Popova, E.; Del Cardayre, S. B. *Science* **2010**, *329*, 559-562.
3. Lee, S. W.; Keeney, D. R.; Lim, D. H.; Dispirito, A. A.; Semrau, J. D. *Appl. Environ. Microbiol.* **2006**, *72*, 7503-7509.
4. Yang, B.; Hodgkinson, A.; Millward, B. A.; Demaine, A. G. *Int. J. Diabetes Mellitus* **2010**, *2*, 169-174.
5. Shao, J.; Zhou, B.; Chu, B.; Yen, Y. *Curr. Cancer Drug Targets* **2006**, *6*, 409-431.
6. Solomon, E. I.; Brunold, T. C.; Davis, M. I.; Kemsley, J. N.; Lee, S. K.; Lehnert, N.; Neese, F.; Skulan, A. J.; Yang, Y. S.; Zhou, J. *Chem. Rev.* **2000**, *100*, 235-349.
7. Andrews, S. C. *Biochim. Biophys. Acta* **2010**, *1800*, 691-705.
8. Theil, E. C. *J. Nutr.* **2003**, *133*, 1549S-1553S.
9. Fang, H.; Caranto, J. D.; Mendoza, R.; Taylor, A. B.; Hart, P. J.; Kurtz, D. M., Jr. *J. Biol. Inorg. Chem.* **2012**, *17*, 1231-1239.
10. Kurtz, D. M., Jr. *Dalton Trans.* **2007**, *0*, 4115-4121.
11. Hayashi, T.; Caranto, J. D.; Wampler, D. A.; Kurtz, D. M., Jr.; Moënné-Loccoz, P. *Biochemistry* **2010**, *49*, 7040-7049.
12. Silaghi-Dumitrescu, R.; Kurtz, D. M., Jr.; Ljungdahl, L. G.; Lanzilotta, W. N. *Biochemistry* **2005**, *44*, 6492-6501.
13. Jin, S.; Kurtz, D. M., Jr.; Liu, Z. J.; Rose, J.; Wang, B. C. *Biochemistry* **2004**, *43*, 3204-3213.
14. Shiba, T.; Kido, Y.; Sakamoto, K.; Inaoka, D. K.; Tsuge, C.; Tatsumi, R.; Takahashi, G.; Balogun, E. O.; Nara, T.; Aoki, T.; Honma, T.; Tanaka, A.; Inoue, M.; Matsuoka, S.; Saimoto, H.; Moore, A. L.; Harada, S.; Kita, K. *Proc. Natl. Acad. Sci. U. S. A.* **2013**, *110*, 4580-4585.
15. Whittington, D. A.; Lippard, S. J. *J. Am. Chem. Soc.* **2001**, *123*, 827-838.
16. Mitić, N.; Schwartz, J. K.; Brazeau, B. J.; Lipscomb, J. D.; Solomon, E. I. *Biochemistry* **2008**, *47*, 8386-8397.

17. Lipscomb, J. D. *Annu. Rev. Microbiol.* **1994**, *48*, 371-399.
18. Baik, M. H.; Newcomb, M.; Friesner, R. A.; Lippard, S. J. *Chem. Rev.* **2003**, *103*, 2385-2420.
19. Bertrand, E.; Sakai, R.; Rozhkova-Novosad, E.; Moe, L.; Fox, B. G.; Groves, J. T.; Austin, R. N. *J. Inorg. Biochem.* **2005**, *99*, 1998-2006.
20. Choi, Y. S.; Zhang, H.; Brunzelle, J. S.; Nair, S. K.; Zhao, H. *Proc. Natl. Acad. Sci. USA* **2008**, *105*, 6858-6863.
21. Winkler, R.; Hertweck, C. *Angew. Chem. Int. Ed. Engl.* **2005**, *44*, 4083-4087.
22. Wei, P. P.; Skulan, A. J.; Mitić, N.; Yang, Y. S.; Saleh, L.; Bollinger, J. M., Jr.; Solomon, E. I. *J. Am. Chem. Soc.* **2004**, *126*, 3777-3788.
23. Lindqvist, Y.; Huang, W.; Schneider, G.; Shanklin, J. *EMBO J.* **1996**, *15*, 4081-4092.
24. Yang, Y. S.; Broadwater, J. A.; Pulver, S. C.; Fox, B. G.; Solomon, E. I. *J. Am. Chem. Soc.* **1999**, *121*, 2770-2783.
25. Stubbe, J. *Curr. Opin. Chem. Biol.* **2003**, *7*, 183-188.
26. Xing, G.; Hoffart, L. M.; Diao, Y.; Prabhu, K. S.; Arner, R. J.; Reddy, C. C.; Krebs, C.; Bollinger, J. M., Jr. *Biochemistry* **2006**, *45*, 5393-5401.
27. Simurdiak, M.; Lee, J.; Zhao, H. *ChemBioChem* **2006**, *7*, 1169-1172.
28. Krebs, C.; Matthews, M. L.; Jiang, W.; Bollinger, J. M., Jr. *Biochemistry* **2007**, *46*, 10413-10418.
29. Li, N.; Korboukh, V. K.; Krebs, C.; Bollinger, J. M., Jr. *Proc. Natl. Acad. Sci. USA* **2010**, *107*, 15722-15727.
30. Brown, P. M.; Caradoc-Davies, T. T.; Dickson, J. M.; Cooper, G. J.; Loomes, K. M.; Baker, E. N. *Proc. Natl. Acad. Sci. USA* **2006**, *103*, 15032-15037.
31. Thorsell, A. G.; Persson, C.; Voevodskaya, N.; Busam, R. D.; Hammarstrom, M.; Graslund, S.; Graslund, A.; Hallberg, B. M. *J. Biol. Chem.* **2008**, *283*, 15209-15216.
32. Liu, K. E.; Wang, D.; Huynh, B. H.; Edmondson, D. E.; Salifoglou, A.; Lippard, S. J. *J. Am. Chem. Soc.* **1994**, *116*, 7465-7466.
33. Tong, W. H.; Chen, S.; Lloyd, S. G.; Edmondson, D. E.; Huynh, B. H.; Stubbe, J. *J. Am. Chem. Soc.* **1996**, *118*, 2107-2108.

- 1
2
3 34. Bollinger, J. M., Jr.; Krebs, C.; Vicol, A.; Chen, S.; Ley, B. A.; Edmondson, D. E.; Huynh,
4 B. H. *J. Am. Chem. Soc.* **1998**, *120*, 1094-1095.
5
6
7 35. Yun, D.; Garcia-Serres, R.; Chicalese, B. M.; An, Y. H.; Huynh, B. H.; Bollinger, J. M., Jr.
8 *Biochemistry* **2007**, *46*, 1925-1932.
9
10 36. Broadwater, J. A.; Ai, J.; Loehr, T. M.; Sanders-Loehr, J.; Fox, B. G. *Biochemistry* **1998**, *37*,
11 14664-14671.
12
13
14 37. Pereira, A. S.; Small, W.; Krebs, C.; Tavares, P.; Edmondson, D. E.; Theil, E. C.; Huynh, B.
15 H. *Biochemistry* **1998**, *37*, 9871-9876.
16
17
18 38. Korboukh, V. K.; Li, N.; Barr, E. W.; Bollinger, J. M., Jr.; Krebs, C. *J. Am. Chem. Soc.* **2009**,
19 *131*, 13608-13609.
20
21 39. Murray, L. J.; Garcia-Serres, R.; Naik, S.; Huynh, B. H.; Lippard, S. J. *J. Am. Chem. Soc.*
22 **2006**, *128*, 7458-7459.
23
24
25 40. Tinberg, C. E.; Lippard, S. J. *Acc. Chem. Res.* **2011**, *44*, 280-288.
26
27
28 41. Ambundo, E. A.; Friesner, R. A.; Lippard, S. J. *J. Am. Chem. Soc.* **2002**, *124*, 8770-8771.
29
30 42. Beauvais, L. G.; Lippard, S. J. *Biochem. Biophys. Res. Commun.* **2005**, *338*, 262-266.
31
32 43. Nordlund, P.; Eklund, H. *J. Mol. Biol.* **1993**, *232*, 123-164.
33
34 44. Calhoun, J. R.; Liu, W.; Spiegel, K.; Dal Peraro, M.; Klein, M. L.; Valentine, K. G.; Wand,
35 A. J.; DeGrado, W. F. *Structure* **2008**, *16*, 210-215.
36
37 45. DeGrado, W. F.; Summa, C. M.; Pavone, V.; Nastri, F.; Lombardi, A. *Annu. Rev. Biochem.*
38 **1999**, *68*, 779-819.
39
40 46. Bryson, J. W.; Betz, S. F.; Lu, H. S.; Suich, D. J.; Zhou, H. X.; O'Neil, K. T.; DeGrado, W.
41 F. *Science* **1995**, *270*, 935-941.
42
43
44 47. DeGrado, W. F.; Wasserman, Z. R.; Lear, J. D. *Science* **1989**, *243*, 622-628.
45
46
47 48. Bell, C. B. III; Calhoun, J. R.; Bobyr, E.; Wei, P.; Hedman, B.; Hodgson, K. O.; DeGrado,
48 W. F.; Solomon, E. I. *Biochemistry* **2009**, *48*, 59-73.
49
50 49. Calhoun, J. R.; Kono, H.; Lahr, S.; Wang, W.; DeGrado, W. F.; Saven, J. G. *J. Mol. Biol.*
51 **2003**, *334*, 1101-1115.
52
53
54 50. Calhoun, J. R.; Bell, C. B. III; Smith, T. J.; Thamann, T. J.; DeGrado, W. F.; Solomon, E. I.
55 *J. Am. Chem. Soc.* **2008**, *130*, 9188-9189.
56
57
58
59
60

- 1
2
3 51. Reig, A. J.; Pires, M. M.; Snyder, R. A.; Wu, Y.; Jo, H.; Kulp, D. W.; Butch, S. E.; Calhoun,
4 J. R.; Szyperki, T.; Solomon, E. I.; DeGrado, W. F. *Nat. Chem.* **2012**, *4*, 900–906.
5
6
7 52. Snyder, R. A.; Betzu, J.; Butch, S. E.; Reig, A. J.; DeGrado, W. F.; Solomon, E. I. *Submitted*
8 *to Biochemistry*.
9
10 53. Kaplan, J.; DeGrado, W. F. *Proc. Natl. Acad. Sci. USA* **2004**, *101*, 11566-11570.
11
12 54. Tang, H. T.; Lunte, C. E.; Halsall, H. B.; Heineman, W. R. *Anal. Chim. Acta* **1988**, *214*, 187-
13 195.
14
15 55. Safavi, A.; Maleki, N.; Moradlou, O. *Electroanal* **2008**, *20*, 2158-2162.
16
17 56. Park, K.; Li, N.; Kwak, Y.; Srnec, M.; Bell, C. B., III; Liu, L. V.; Wong, S. D.; Yoda, Y.;
18 Kitao, S.; Seto, M.; Hu, M.; Zhao, J.; Krebs, C.; Bollinger, J. M., Jr.; Solomon, E. I. *In*
19 *Preparation*.
20
21
22
23
24
25
26
27
28
29
30
31
32
33
34
35
36
37
38
39
40
41
42
43
44
45
46
47
48
49
50
51
52
53
54
55
56
57
58
59
60

TOC graphic

